https://doi.org/10.5194/acp-2020-57
Preprint. Discussion started: 16 April 2020

Atmospheric Chemistry and Physics Discussions

Models transport Saharan dust too low in the atmosphere compared to observations

Debbie O'Sullivan[1], Franco Marenco[1], Claire L. Ryder[2], Yaswant Pradhan[1], Zak Kipling[3], Ben Johnson[1], Angela Benedetti[3], Melissa Brooks[1], Matthew McGill[4], John Yorks[4], Patrick Selmer[4]

[1]Met Office, Exeter, EX1 3PB, UK
[2]Department of Meteorology, University of Reading, RG6 6BB, UK
[3]European Centre for Medium-Range Weather Forecasts, Reading, RG2 9AX, UK
[4]NASA Goddard Space Flight Center, Greenbelt, MD 20771, USA

Correspondence to: Franco Marenco (franco.marenco@metoffice.gov.uk)

Abstract. We investigate the dust forecasts from two operational global atmospheric models in comparison with in-situ and remote sensing measurements obtained during the AERosol properties – Dust (AER-D) field campaign. Airborne elastic backscatter lidar measurements were performed on-board the Facility for Airborne Atmospheric Measurements during August 2015 over the Eastern Atlantic, and they permitted to characterize the dust vertical distribution in detail, offering insights on transport from the Sahara. They were complemented with airborne in-situ measurements of dust size-distribution and optical properties, and datasets from the Cloud-Aerosol Transport System spaceborne lidar (CATS) and the Moderate Resolution Imaging Spectroradiometer (MODIS). We compare the airborne and spaceborne datasets to operational predictions obtained from the Met Office Unified Model (MetUM) and the Copernicus Atmosphere Monitoring Service (CAMS). The dust aerosol optical depth predictions from the models are generally in agreement with the observations, but display a low bias. However, the predicted vertical distribution places the dust lower in the atmosphere than highlighted in our observations. This is particularly noticeable for the MetUM, which does not transport coarse dust high enough in the atmosphere, nor far enough away from source. We also found that both model forecasts underpredict coarse mode dust, and at times overpredict fine mode dust. An analysis of the processes driving dust uplift in the models suggests that errors in the large scale wind and dust size distribution at source could be the cause of differences between model predictions and observations of the Saharan Air Layer. Mineral dust is an important component of the climate system, therefore it is important to assess how models reproduce its properties and transport mechanisms.

1 Introduction

Mineral dust is an important component of the Earth system (Forster et al., 2007, Haywood and Boucher, 2010, Knippertz and Todd, 2012), and it affects the scattering and absorption of solar and infrared radiation, as well as cloud microphysics. The Saharan desert is the main source of mineral dust (Washington et al., 2003; Shao et al., 2011), and once lifted into the air the dust can be transported over thousands of kilometres (Knippertz and Todd, 2012., Tsamalis et al., 2013) where it is exposed to the effects of ageing and mixing. These effects change its optical, microphysical and cloud condensation properties (Richardson et al., 2007., Lavaysse et al., 2011),

https://doi.org/10.5194/acp-2020-57
Preprint. Discussion started: 16 April 2020


Atmospheric Chemistry and Physics Discussions

affecting the size distribution, the chemical composition, and the radiative effects. The transported dust also affects tropical cyclone development through effects on the sea surface temperature (Evan et al., 2018), and the deposition of iron-rich material into the ocean has an impact on biogeochemical cycles (Jickells et al., 2005).

Dust is forecast prognostically in Numerical Weather Predictions (NWP) because of its impacts on atmospheric circulation (Mulcahy et al., 2014; Solomos et al., 2011), visibility, air quality, health and aviation. Significant progress has been made in dust modelling over the last decade, with a suite of regional and global dust models now available. In recent years dust models have also started to assimilate aerosol optical depth (AOD) measurements from satellites (Niu et al., 2008; Benedetti et al, 2009; Liu et al., 2011; Di Tomaso et al, 2017). There have been a number of studies in recent years to provide further insight on the transport and properties of dust (e.g. Heintzenberg, 2009, Ansmann et al., 2011, Kanitz et al., 2014, Ryder et al., 2015, Groβ et al., 2015 among many more), and the ability of models to predict dust events (e.g. Chouza et al., 2016, Ansmann et al., 2017.) However, there have been few studies assessing how well the vertical distribution of dust is captured in models. For example, Chouza et al., (2016) found that the ECMWF MACC model (precursor to the CAMS model considered here) simulated Saharan plumes that matched the observations, but underestimated the marine boundary layer aerosol. More recently, Ansmann et al., (2017) found that dust models, including the one run at ECMWF, were able to forecast dust well for the first few days after emission, but that the modelled loss processes were too strong, leading to an underestimation with increasing distance from source. Other studies have shown that dust is not optimally represented in models, highlighting insufficient uplift and insufficient transport of the coarser particles. For example, Evan (2018) found that the representation of dust in climate models was affected by errors in the surface wind fields over Northern Africa. Given the diversity of findings and the range of available models and methodologies, there is a continued need to assess the model predictions of the dust vertical distribution.

Aerosol Robotic Network (AERONET) sun photometer retrievals (Holben et al., 1998) play an important role in dust model evaluation (for example see: Scanza et al., 2015; Cuevas et al., 2015; Ridley et al, 2016) and offer near continuous measurements and, for some stations, long observation records. However, AERONET instruments do not provide information on vertical distribution. Dry convective mixing can raise mineral dust to altitudes of at least 5-6 km over the Sahara, and disperse it into a deep mixed layer (Messager et al., 2010). The dominant Easterly winds at these latitudes advect this airmass across the Atlantic Ocean, and as the hot, dry and dust-laden air passes the West African coast, it is undercut by cooler moist air in the marine boundary layer (MBL) and forms an elevated layer called the Saharan Air Layer (SAL) (Karyampudi et al., 1999). As plumes move across the Atlantic, the altitude of the SAL may decline due to large-scale subsidence and loss processes, and the residence time of the lofted dust is closely related to the height and size distributions. The impact of dust on radiation and clouds also depend on its vertical distribution (Johnson et al., 2008). The key loss processes, wet and dry deposition and turbulent downward mixing, are strongly influenced by the altitude of the dust and the fine and coarse mode fractions. Note that in this paper we will denote particles with diameters < 1 μm as fine mode dust, with coarse mode particles having diameters >1 μm.

https://doi.org/10.5194/acp-2020-57
Preprint. Discussion started: 16 April 2020


Atmospheric Chemistry and Physics Discussions

Lidar observations provide valuable information about the location and vertical distribution of aerosols in the atmosphere, and can as such be useful in the evaluation dust models. Spaceborne lidar measurements provide this information on a global scale. For example, the Cloud-Aerosol Lidar with Orthogonal Polarization (CALIOP) on board the Cloud-Aerosol Lidar and Infrared Pathfinder Satellite Observations (CALIPSO) is an elastic backscatter lidar system (Winker et al., 2010) with limited capability to distinguish different types of aerosol (Omar et al., 2009). The Cloud-Aerosol Transport System (CATS) onboard the International Space Station was a polarisation sensitive backscatter lidar with higher detection sensitivity than CALIOP and superior ability to differentiate different aerosol types (Yorks et al., 2016). Both systems include depolarisation measurements, which permits the identification of mineral dust reliably vs other aerosol types. Airborne lidar measurements of aerosols typically offer a finer resolution and the combination with a number of other airborne instruments, but on a limited geographical scale (see e.g. Marenco et al, 2011; Marenco, 2013; Marenco et al, 2016).

In this work we compare airborne measurements of mineral dust with model predictions. The measurements include remote sensing with elastic-backscatter lidar and in-situ dust observations of the particle size distribution. We also make use of data from the CATS spaceborne lidar to extend our analysis over the Sahara. The observations are used to assess the performance of the dust forecast from two operational global models, the Met Office Unified Model (MetUM) and the European Centre for Medium-range Weather Forecasts, Copernicus Atmosphere Monitoring Service (ECMWF-CAMS) model. The data are used to investigate whether convection, largescale wind, boundary layer height, or dust size distribution have the greatest effect on how well the models capture the vertical structure of the dust layers.

2 Models

In this study observation data is used to assess the relative performance of the dust schemes in two operational global models. Both models and their respective dust schemes are briefly described in section 2.1 and 2.2. Both models considered here assimilate MODIS AOD into the model analysis to improve the AOD forecast (e.g Pope et al., 2016), and the models perform generally well for the prediction of dust AOD. For this study, short range forecasts were used (forecast lead time < 12 hours).

2.1 MetUM

The Met Office Unified Model (MetUM) is a non-hydrostatic, fully compressible, deep-atmosphere dynamical core, solved with a semi-implicit semi-Lagrangian time step on a regular latitude-longitude grid (Davis et al., 2005). The configuration used in this study is the Global NWP model that was operational in 2015 (Global Atmosphere 6.1), which had a resolution of 0.35° longitude by 0.23° latitude, corresponding to an approximate resolution of 25 km at mid-latitudes and ~40 km at the equator (Walters et al, 2017). There are 70 vertical levels, reaching an altitude of 80 km (Pope et al., 2016). The dust scheme uses 9 size bins for the horizontal flux calculations with diameters between 0.0632 μm to 2000 μm, and either a 6 or 2 bin scheme for the subsequent transport and advection (Woodward 2001; Woodward 2011; Collins et al., 2011; Brooks et al, 2011). The

https://doi.org/10.5194/acp-2020-57
Preprint. Discussion started: 16 April 2020


Atmospheric Chemistry and Physics Discussions

operational Global model, used here, uses the 2-bin dust scheme, with a fine and accumulation mode bin (division 1 or d1, 0.2 - 4.0 µm diameter) and a coarse mode bin: (division 2 or d2, 4.0 - 20 µm diameter).

AOD from MODIS collection 5 on-board the Aqua satellite was assimilated into the model, from Deep Blue and Dark Target-Land retrievals, and Dark Target-Ocean retrievals over selected ocean regions. There are four daily model runs, initialised at 00, 06, 12 and 18 UTC, and the model fields are available with a timestep of 3 hours (00, 03, 06, 09, 12, 15, 18 and 21 UTC). See Pope et al., (2016) and references therein for a description of how the model is initialised and the AOD data assimilation methodology.

2.2 ECMWF – CAMS

The global atmospheric composition forecasts run at ECMWF, as part of the Copernicus Atmospheric Monitoring Service (CAMS), are a continuation of the work of the Monitoring Atmospheric Composition and Climate (MACC) project. The CAMS system combines state-of-the-art modelling with Earth observation data assimilated from a variety of sources, including MODIS AOD. The data used here are from the operational forecasts produced in near real time during the period of the ICE-D campaign. At that time, the horizontal resolution was 80km (corresponding to a T255 spectral truncation) and there were 60 vertical levels. The model provided a 120 h long forecast from 00UTC, and the analysis used 12-hourly 4D-VAR data assimilation, using MODIS Terra and Aqua Dark Target AOD to constrain the total aerosol mixing ratio. Details of the model set up and the analyses can be found in Morcrette et al., (2009), Benedetti et al., (2009), and Cuevas et al., (2015). The operational CAMS global assimilation and forecasting system uses fully integrated chemistry in the ECMWF Integrated Forecasting System (IFS), for this time period cycle 40r2. The IFS is a spectral model using vorticity-divergence formulation with semi-Lagrangian advection and physical parameterizations on a reduced Gaussian grid. The CAMS aerosol parameterization is based on the LOA/LMD-Z (Laboratoire d-Optique Atmosphérique/Laboratoire de Météorologie Dynamique-Zoom) model (Reddy et al., 2005). Prognostic aerosol of natural origin such as mineral dust and sea salt are described using three size bins. In total CAMS has 5 different types of prognostic aerosol, unlike the MetUM which only has dust in the operational model. For dust the bin size classes are one fine mode (division 1 or d1, 0.06-1.1 µm diameter), and two coarse mode bins (division 2 or d2: 1.1-1.8 µm diameter, and division 3 or d3: 1.8-40 µm diameter). Morcrette et al., (2009) state that the size bins are chosen such that the mass concentration percentages are 10% for the fine dust mode, and 20% and 70% for the two coarse dust size bins during emission.

3 Measurements and instrumentation

3.1 ICE-D campaign

AERosol properties – Dust (AER-D) was a collaborative campaign led by the Met Office in collaboration with the Universities of Reading and Hertfordshire (Marenco et al, 2018). It was held at the same time as the Ice in Clouds Experiment – Dust (ICE-D), a larger collaborative campaign involving the Met Office, the, National Centre for Atmospheric Science (NCAS), Manchester and Leeds Universities (UK), the British Antarctic Survey

https://doi.org/10.5194/acp-2020-57
Preprint. Discussion started: 16 April 2020

Atmospheric Chemistry and Physics Discussions

and Mainz University. In addition, the Sunphotometer Airborne Validation Experiment in Dust (SAVEX-D) was also carried out, thanks to EUFAR funding based on a proposal from the University of Valencia, Spain, the Met Office and the University of Reading. SAVEX-D is treated here as a component of AER-D. The AER-D and ICE-D field campaigns were conducted on 6-25 August 2015 from Praia, Cape Verde (14°57'N, 23°29'W), 650 km off the West coast of Africa, an ideal region for observing dust outflow. The main aim of the ICE-D campaign was to characterise the properties of Saharan dust as ice nuclei (IN) and cloud condensation nuclei (CCN), their impact on cloud microphysical processes, and the formation of convective and stratiform clouds. The AER-D and SAVEX-D projects aimed at characterizing dust properties above the Eastern Atlantic. The main measurements were made using the Facility for Atmospheric Airborne Measurements (FAAM) Airborne Research Aircraft, a modified BAe-146-301, and in total, 16 flights took place between both campaigns, six of which contained high-altitude sections dedicated to surveying the vertical distribution of dust using lidar. The instruments deployed on the aircraft enabled a range of measurements of aerosol size distribution, chemical composition, optical properties and radiative effects. Most flights took place in proximity of the Cape Verde Islands, with the exception of flights B923, B924 and B932, which sampled between Cape Verde and the Canaries. Ground-based measurements were also made on the island of Santiago during the month. These experiments together provide a comprehensive dataset to investigate the properties of transported Saharan dust during the summer season. The key airborne instruments, and satellite data used in this study are briefly discussed in the next sections.

During AER-D and ICE-D, Saharan air masses were transported by predominantly Easterly winds over the Atlantic in a sequence of events between the 6th and 25th August. Cape Verde was often on the edge of the transported dust, enabling flights to sample the main dust plume and a gradient across the flight track. The dust episodes often lasted for several days, which provided the opportunity to make measurements of dust of varying age. Among the key aims of the AER-D project are the improvement of dust remote sensing from space and from the ground, and the validation of dust predictions in the MetUM and other models. The focus of the present paper is on the latter objective. Four dust events are considered here, derived from five research flights (one event having been sampled through a double flight). A summary of the flight sections considered is given in Tables 1 and 2, and the flight tracks are shown in Fig 1. We use these data to investigate whether convection, largescale wind, boundary layer height, or dust size distribution have the greatest effect on how well the models capture the vertical structure of the dust layers. There is no direct measure for convection in the archived model fields, as such the impact of convection on the dust forecast can only be inferred through a process of elimination.

For convenience flight sections are divided in "runs" and "profiles": we have a run (also called straight and level run, and denoted here with the letter R) when the aircraft flies for a certain time on a constant heading and a constant altitude, and a profile (denoted here with the letter P) when the aircraft changes altitude with a constant rate of ascent or descent. Note that an aircraft profile is a slant trajectory through the atmosphere and thus differs from a lidar profile (vertical). Each aircraft run or profile is identified with a number, hence for a given flight we have R1, R2, … and P1, P2, …. The runs and profiles of interest in this paper are identified in Tables 1 and 2.

https://doi.org/10.5194/acp-2020-57
Preprint. Discussion started: 16 April 2020


Atmospheric Chemistry and Physics Discussions

3.2 Airborne lidar

The Leosphere ALS450 elastic backscatter lidar (wavelength 355 nm) is deployed on the FAAM aircraft in a nadir-viewing geometry. Marenco et al., 2011, and Marenco, 2013 describe the methodology for converting lidar beam returns at 355 nm wavelength into profiles of aerosol extinction coefficient. The system specifications are summarised in Marenco et al., 2014 and references therein, and a further description of the data processing methodology can be found in Marenco et al., 2016. During processing, the lidar data was integrated to 1 min temporal resolution, which corresponds to a 9 ± 2 km footprint at typical aircraft speeds. Smoothing to a 45 m vertical resolution was also applied to reduce the effect of shot noise. The vertical profiles were processed using a double iteration. First we determined the lidar ratio (extinction-to-backscatter ratio), and subsequently we processed the full data set to determine the extinction coefficient and AOD (see Marenco et al., 2016 and references therein, where the same methodology is applied). The first iteration was conducted on a subset of the vertical profiles, where the signature of Rayleigh scattering above the dust layer could clearly be identified to enable the lidar ratio to be determined. We obtained a campaign mean lidar ratio of 54 ± 8 sr, which is in reasonable agreement with other measurements of the lidar ratio for dust at 355 nm (Lopes et al., 2013). This value of the lidar ratio was subsequently used to process the full dataset in the second iteration. On average during this campaign, the uncertainty in the derived dust extinction coefficient was 8%; however with a significant variability of this figure in both the vertical and horizontal. The uncertainty is smaller than this near the top of the profile (closer to the aircraft) and larger nearer the ground. The methodology described in Marenco et al., (2016) was used here.

3.3 In-situ aerosol measurements

A number of wing-mounted instruments permitted us to measure the aerosol size distribution between 0.1 and 100 µm. The Passive Cavity Aerosol Spectrometer Probe (PCASP; Liu et al., 1992; Osborne et al., 2008; Rosenberg et al., 2012) measured optical size from 0.1-2.5µm. The cloud droplet probe (CDP-100; Lance et al., 2010; Rosenberg et al., 2012) measured larger particles with diameters 5-40 µm (Knollenberg, 1981), and the two-dimensional stereo probe (2DS) measured large aerosol particles up to ~100 µm. Calibration of the PCASP was done before and after the campaign, whereas the CDP was also calibrated before most flights. The PCASP and CDP measurements (d <20 µm) and their calibration for the ICE-D campaign are discussed in more detail in Ryder et al (2018), where the full size distribution measurements are described. The particle size spectra have been processed for an assumed refractive index for dust of 1.53−0.001i, thus correcting for the bin ranges calibrated using polystyrene latex spheres, and the first bin has been discarded due to its undefined lower edge. The 2DS is a shadowing probe with 10 µm resolution, and it does not rely on refractive index to infer particle size. Profiles of in situ measurements were acquired on slant trajectories through the atmosphere (aircraft profiles).

3.4 Satellite data

Two sources of satellite data are used here, the Cloud-Aerosol Transport System (CATS) and the Moderate Resolution Imaging Spectroradiometer (MODIS). CATS is a multi-wavelength lidar instrument (wavelengths 532

https://doi.org/10.5194/acp-2020-57
Preprint. Discussion started: 16 April 2020


Atmospheric Chemistry and Physics Discussions

and 1064 nm) developed to enhance Earth Science remote sensing capabilities from the International Space Station (ISS) (McGill et al., 2015).

MODIS collection 6.1 level-2 atmospheric aerosol product from Aqua (MYD04_L2) and Terra (MOD04_L2) were obtained from the Level-1 and Atmosphere Archive & Distribution System (LAADS, ftp://ladsftp.nascom.nasa.gov/allData/61/). The merged Deep Blue and Dark Target aerosol optical depth at 550 nm from both Aqua and Terra was used to create daily AOD maps (Hsu et al, 2004, 2006, 2013; Levy et al, 2013; Sayer et al, 2013, 2014).

3.5 Analysis of dust source regions and transport

Source regions for the sampled dust were investigated using two backtrajectory models. Back-trajectories were calculated from the time, latitude, longitude and altitude of various points along the flight track where high dust loadings had been encountered, using the Numerical Atmospheric Modelling Environment (NAME) (Jones et al, 2007) and the Hybrid Single-Particle Lagrangian Integrated Trajectory model (HYSPLIT) (Draxler and Hess, 1998; Stein et al, 2015), resulting in consistent source regions between the two models.

Haboobs driven by convective outflows from mesoscale storms have been shown to represent the dominant uplift mechanism of Saharan dust during the summer months, with a share of 50% of the uplifted dust (Marsham et al., 2013). The meteorological reanalyses driving HYSPLIT back-trajectories and NAME dosage maps are not able to identify the dust source location, or potentially the transport pathways over these or subsequent uplift events (Sodemann et al., 2015). On the other hand, haboobs and dust storms are clearly identified by an expert eye in the EUMETSAT "dust RGB" product from the MSG/SEVIRI infrared channels (http://oiswww.eumetsat.int/~idds/html/product_description.html), and it is thus possible to utilise this type of imagery to track dust as it is transported, thus helping to determine source location and uplift time (e.g Schepanski et al., 2007). Dust events observed during four of the flights considered here were examined in this way by Ryder et al. (2018) and mesoscale convective storms drove the dust uplift and subsequent transport in all of them. Despite the inability of back trajectory analysis to really capture haboobs, the backtrajectories and the satellite-tracking of the plumes gave consistent results.

The identified source regions and dust transport paths are shown in Fig 1. This uses a combination of work done by Ryder et al. (2018) and Liu et al. (2018), with additional information in this work from NAME and HYSPLIT to help identify the dust trajectory. A detailed discussion on the meteorology during the ICE-D campaign can be found in Liu et al, (2018). A key point is that the MBL in the Eastern Atlantic was typically 300 – 500 m deep during the study period, which is in agreement with the aircraft lidar observations and the in-situ measurements during aircraft ascent and descent profiles. Liu et al., (2018) also show that on the 15th of August there was a change in the synoptic conditions. This means that for the first and third case study used here (B920 and B927) the maximum horizontal wind speed above the MBL, in the Saharan Air Layer (SAL) was lower than 10 m/s and wind direction varied between NE and SE which resulted in lower dust loadings during these two flights. Case study 2 (B923 and B924) was also in this period of slower windspeeds, but high dust loadings were sampled due to the more northerly location of flights B923 and B924. In the final case study looked at here, case study 4

https://doi.org/10.5194/acp-2020-57
Preprint. Discussion started: 16 April 2020


Atmospheric Chemistry and Physics Discussions

(B932), the wind speed above 2km was significantly enhanced with a more Easterly wind direction. This resulted in higher dust loadings being observed in case study 4 than for 1 or 3 – note that the highest dust loadings of all were observed in case study 2 due to the location of these flights, see Liu et al., (2018) for the full meteorological and dust source analysis.

3.6 Comparison of datasets

The airborne lidar measurements of aerosol extinction coefficient and AOD were measured at a wavelength of 355 nm, whereas the MODIS and AERONET data used here were all collected at 550 nm, and CATS aerosol properties are at 1064 nm. The model extinction is available for a variety of wavelengths including 380, 550 and 1064 nm, and for CAMS 355 nm is also available. Here, the MetUM dust aerosol extinction coefficient was re-calculated from the mass concentrations of division 1 and division 2 dust (see section 2.1 for a description of the dust scheme), and Mie-derived optical properties of the two dust size bins.

Where model and observation (e.g AERONET) data were available for more than one wavelength, very little wavelength dependence was noted. This is explained with the small Ångström exponent during the campaign (-0.4 to 0.4) (see Liu et al., 2018), and this is generally expected for coarse mineral dust particles. For this reason, it was deemed unnecessary to account for wavelength-dependence in the present study. Airborne lidar and model extinction coefficient measurements are all shown for 355 nm, whereas MODIS and AERONET AOD is at 550 nm, and the CATS data is at 1064 nm. In section 4.1 (fig 16-19), model data are shown at 1064 nm in comparison with CATS, but as already highlighted there is virtually no difference between the extinction at 355 and 1064.

The MetUM extinction coefficient only includes dust, which could potentially make the results lower compared to total aerosol extinction which also includes other aerosol types. However, data from the CATS lidar, as well as the in-situ measurements including filter samples discussed in Ryder et al (2018), confirm that the aerosol sampled during AER-D/ICE-D was predominantly dust, with a contribution from marine aerosol in the MBL. For this reason, for this study we neglect the conceptual difference between the dust-only extinction of the MetUM, and total-aerosol properties in CAMS and the observations.

4 Results and discussion

In sections 4.1 and 4.2, the measurements of aerosol extinction coefficient, AOD and dust concentration for the different size bins used by the MetUM and CAMS are used to assess the predicted dust, as well as the representation of dust size distribution in both models. In sections 4.3 and 4.4, the model largescale wind and boundary layer height are compared with observations to infer what if any influence these have on the dust forecast.

https://doi.org/10.5194/acp-2020-57
Preprint. Discussion started: 16 April 2020


Atmospheric Chemistry and Physics Discussions

4.1 Individual case studies

285 **Case study 1: 7th August 2015, B920 (Fig 2 - 7).** This flight took place near Praia and was co-located with an overpass of the CATS spaceborne lidar. There were two high level sections during the flight that have been looked at, R1 and R6 (see Table 1 for run times and locations). Fig 2 displays the airborne, spaceborne and model data for R6, which coincided with a CATS overpass. A deep dust layer was observed between ~ 2 and 5 km, with marine aerosol mixed with dust in the boundary layer, and a broken cloud field at the top of the boundary
290 layer. Both the extent and amount of aerosol observed agree well between the airborne and the spaceborne lidars (Fig 2 a and d). The aerosol type classification from CATS (not shown here) also agrees well with the in-situ measurements, which found a marine aerosol layer below the dust layer. The dust layer was well mixed, with moderate extinction coefficients (100 - 180 Mm^{-1}) and AOD's between 0.28 and 0.44 observed by the airborne lidar.

295 Fig 2e-g show that the AOD from the two lidars agrees well with both models around Cape Verde, with much larger values predicted by both models near the Canary Islands. The AOD observations from MODIS, AERONET (stars) and the aircraft lidar (dots) are in agreement. The spatial distribution of the AOD in both models over West Africa and just off the coast, is broadly in agreement with the MODIS and AERONET observations, and this is consistent with the fact that both models assimilate MODIS AOD. However, the models
300 under-predict the intensity of the AOD maximum, and there are also variations in the predicted plume location.

From Fig 2a-d we see that the predicted vertical distribution of the dust layer shows some differences from the observations: the dust layer extends from the surface to around 4 km in the MetUM and from 1 to ~ 4 km in CAMS, whereas CATS and the airborne lidar both show the dust layer between 2 and 5 km. The magnitude of the extinction coefficient predicted by the models of 100 – 120 Mm^{-1} is however in good agreement with the
305 observations. The mean, standard deviation and maximum extinction values for each considered flight section are summarised in Table 1. For this run, the MetUM mean extinction was 55± 38 Mm^{-1}, ECMWF forecast 58± 41 Mm^{-1} and the aircraft lidar measured a mean extinction value of 56± 40 Mm^{-1}.

In Fig 3a the mean extinction profile for R6 is shown for the airborne lidar, the MetUM and the CAMS model, and Fig 3b displays the mean dust concentration profile in each of the size bins for both models for the same time
310 period. As already highlighted from Fig 2, the MetUM has the dust layer extending right down to the ocean surface. It is moreover dominated by the smaller size bin (d1, 0.2 – 4.0 µm diameter), in particular for the aerosol below 1km primarily. The concentration predicted by CAMS for this case is less than half of that in the MetUM, and however the magnitude of the predicted extinction is similar, although with differences in the dust layering.

The dust concentration from the MetUM divisions d1 and d2 and the CAMS divisions d1 (0.06-1.1 µm diameter),
315 d2 (1.1-1.8 µm diameter), and d3 (1.8-40 µm diameter) have also been compared with the in-situ measurements for each of the 5 size ranges, as well as the total dust concentration measured during aircraft profiles. Two profiles from this flight are shown in Fig 4 and 5. The observed concentration of dust in the MetUM d1 size bin typically makes up about a third of the total dust concentration measured, and d2 is around two thirds. In contrast, the measurements show very little dust in the CAMS d1 and d2 size bins, and the concentration in the d3 size bin

https://doi.org/10.5194/acp-2020-57
Preprint. Discussion started: 16 April 2020


Atmospheric Chemistry and Physics Discussions

is very close to the total measured. Comparing the model data (lines with markers on) to the measurements (lines of the same colour with no markers) in Fig 4 and 5 we can see that both models struggle to accurately capture dust concentration for each size bin. This adds to the difficulty in attributing dust to the right altitude. For example, in P2 (Fig5a) the MetUM has more d1 dust than d2, while the aircraft measurements show the opposite. For the same profile (Fig 5b), CAMS has more d2 dust than d3, however the measurements show that there is very little d1 or d2 dust, and the predicted CAMS d3 is about a factor of 3 too low.

Temperature and specific humidity profiles from the aircraft in-situ instruments were also compared with data from the MetUM and ECMWF. An example is shown for this flight for P2 (Fig 6) and P7 (Fig 7). The temperature profiles are in good agreement for all profiles looked at, with no systematic bias for either model. Both models also generally get the humidity profiles about right, capturing the main features. Generally, the models predict a correct vertical structure of the atmosphere in terms of thermodynamic profiles; however the predicted dust vertical distribution seems to depart excessively from the thermodynamic structure.

Case study 2: 12th August 2015, B923 and B924 (Fig 8-11). Flights B923 and B924 both took place on the 12th August flying between Praia and Fuerteventura to sample the outflow from a dust uplift event that had happened on the 10th August in Northern Mali. These flights were able to reach the main dust plume, which means that highest AOD's and extinction coefficients of the campaign were measured on this day (Marenco et al, 2018). The two flights sampled the same plume at different times during the day, and only B923 is shown here as results for flight B924 are similar. The AOD measured by the airborne lidar reached 2, with an aerosol extinction coefficient of 100 – 1300 Mm^{-1} near the Western African coast. As in the previous case study, both models captured the spatial distribution of the dust AOD well (Fig 8 d-f), however they also under-predicted the AOD.

For this section of flight B923, both models showed a dust layer up to ~ 5 km, with an enhanced extinction coefficient at 13-17°W, between the surface and 1 km, where the extinction coefficient increases from an average in-layer value of 100-150 Mm^{-1} to 500-700 Mm^{-1} (Fig 8a-b and Fig 9). This spatial distribution along the flight track is similar to the observed one (Fig 8c and 9); however, the maximum dust extinction is observed at ~ 1 km altitude, whereas the models predict it closer to the surface, and the dust maximum extinction coefficient along the flight track was under-predicted in the MetUM and CAMS (Table 1). Two sections of flight B924, on the same day, reinforce these results (not shown here as they are similar to the section just discussed). However, Fig 8d-e shows that there is a difference in the general representation by both models: CAMS captures similar AODs to the ones observed by lidar, however positioned slightly further to the East of the aircraft track, whereas the MetUM underpredicts this dust event's maximum AOD. MODIS (Fig 8f) even suggests higher AODs for this day, than what both models and the aircraft lidar can highlight. The differences between models and observations could possibly be associated to the dust having been uplifted by a strong haboob, for which models may fail to capture the strength of the uplift (Roberts et al., 2018).

In P1 the measurements show very large amounts of dust, up to 3000 μg/m^{-3} concentration (Fig 10), with both models predicting an order of magnitude less. Interestingly in this aircraft profile, which is closer to the area affected by the intense dust, both models have the greatest proportion of dust in the largest size bins, in agreement with the in situ measurements.

https://doi.org/10.5194/acp-2020-57
Preprint. Discussion started: 16 April 2020


Atmospheric Chemistry and Physics Discussions

Compared to the very large differences between the measured and modelled dust concentration, the modelled extinction is much closer to the observations.

Case study 3: 15th August, B927 (Fig 11-12). This case study is quite interesting, as the dust was confined to a shallow layer as can be seen in fig 11c. The extinction coefficient (~100 - 300 Mm^{-1}) measured by the lidar, and the AOD (up to 0.36) were moderate. The ECMWF CAMS model does a good job at getting the dust layer in the right vertical level, with comparable aerosol extinction coefficients to the observations, although the predicted layer depth is about double. This is particularly noticeable in the run mean plot (Fig 12a). Whilst the MetUM predicts a dust layer at the correct altitude, the extinction coefficient is under-predicted in this layer and a second dust layer is located lower down in the boundary layer, resulting in a similar AOD (Fig 11b, and 12). The peak altitude of the elevated dust layer is around 2.8 km for both models and the lidar measurements. The ECMWF CAMS model looks closer to the lidar observations, but with a deeper dust layer, whereas the MetUM displays a second dust layer near the surface (Fig 12a).

As has been the case for the two previous examples, the AOD spatial distribution compares well to the combined observations (Fig 11d-f), however the AOD is under-predicted compared to MODIS, particularly by the MetUM. If we look at the mean predicted dust concentration for R1 in Fig 12b both models again have a larger amount of dust in the smaller size bins.

Case study 4: 20th August, B932 (Fig 13 – 15). The fourth case study shows another interesting flight, where the dust was observed in an elevated layer between 2 and 4.5 km (Fig 13c). For the dust observed on this day, the transport time from the source region was shorter compared to the previous three due to larger wind speeds. The dust was uplifted by a mesoscale convective system on the 17th August near the Algeria/Mali border and from the northernmost tip of Mali (Fig 1). The aerosol extinction coefficient (~100 and 400 Mm^{-1}) and AOD observed by the airborne lidar (up to 0.72) were the highest observed during the campaign after B923 and B924. We note that this flight also travelled a considerable distance to the Northeast of Cape Verde, hence getting closer to the main plume. Both models simulate the spatial distribution of the AOD well compared to observations and predict the observed North-South gradient along the flight track. As can be seen from Fig 13a-c both models forecast the top of the dust layer reaching around 4 km, which is only slightly lower than the 4.5 km observed on the lidar. However, the observations show most of the dust in a relatively shallow layer between 2 and 3.5 km, whereas the models have the peak of the dust below 1 km. This can also be seen quite clearly in Fig 14.

Out of the 8 high level sections from the 4 case studies included in this work, R1 from B932 shown here is the only case study where both models predict a higher extinction coefficient than was observed by airborne lidar. As can be seen from Table 1, the lidar measured a mean aerosol extinction coefficient of 76 ± 81 (Max 395 Mm^{-1}), while the MetUM and ECMWF mean and max values were 140 ±130 (Max 620 Mm^{-1}) and 140 ± 120 (Max 500 Mm^{-1}), respectively. In this case, moreover, both models have most of the dust concentration in the largest size bin (Fig 14b), although the fine mode dust still appears overestimated (Ryder et al, 2019). The greater contribution of the smaller dust particles to the extinction coefficient, combined with overestimation of the overall concentration are consistent with the predicted extinction coefficient being higher than the observed one

https://doi.org/10.5194/acp-2020-57
Preprint. Discussion started: 16 April 2020


Atmospheric Chemistry and Physics Discussions

for this case study. Note that the CAMS d2 dust mass concentration of R1 (Fig 14b) and P4 (Fig 15b) is virtually identical to the d3 mass concentration, with the two lines over-lapping.

4.2 General findings from the four case studies considered

For all the case studies the MetUM and ECMWF global dust forecasts capture the spatial distribution of dust AOD reasonably well in comparison with observations. The model predictions show some positioning errors compared to MODIS AOD, and this can affect the local comparisons made at the aircraft location. The models tend to underpredict the AOD, but as shown by case study 4 the opposite can also occur.

The model prediction of the vertical distribution of the dust extinction coefficient is not always consistent with observations. As a general rule, both models tend to have the dust too low in the atmosphere compared with the observations, with ECMWF generally doing a better job at capturing elevated dust layers. In the next section we will use data from the CATS spaceborne lidar, in comparison with predictions from the MetUM, to investigate what could be causing the observed discrepancies in the dust vertical distribution.

We noted very large differences between the measured and modelled dust concentration, associated however with a modelled extinction closer to the observations, which may appear surprising because concentration is the modelled variable, from which optical properties are computed. We need to bear in mind, however, that AOD is the mostly used metric used to compare aerosol model predictions and observations: AERONET AOD is often used in model verification, and both the MetUM and the CAMS model use MODIS AOD in data assimilation. It is not so surprising, therefore, that modelled optical properties are pulled towards the observations, even when the microphysical properties from which they are computed are out of scale (in this case, an underestimated dust concentration). Finer particles make a greater contribution to the aerosol extinction coefficient per unit mass than coarser ones, and the mismatch between the representation in concentration and in optical properties can be compensated in the models through the size-distribution. For all the aircraft profiles studied here, the models have too much of the dust concentration in the smaller size bins, meaning that an underpredicted dust concentration can yield an aerosol extinction coefficient of the right order of magnitude.

For the flights which sampled dust nearer the source regions (case studies 2 and 4) the models had a greater proportion of dust concentration in larger size bins than for the other flights. This seems to indicate that the models may represent the dust size distribution better nearer the source. The observations from the AER-D and ICE-D campaigns suggest that, as the dust travels away, the observed size distribution changes little, with large particles transported in significant quantities as far as Cape Verde (Liu et al., 2018; Ryder et al., 2018). In contrast, the models appear to lose particles from the larger size bins rapidly with increasing dust mass age, due to the gravitational sedimentation processes.

https://doi.org/10.5194/acp-2020-57
Preprint. Discussion started: 16 April 2020

Atmospheric Chemistry and Physics Discussions

4.3. Comparison with the CATS spaceborne lidar

We compared almost every CATS overpass covering North Africa and the Eastern Atlantic during AER-D and ICE-D with the MetUM. CATS and model data were compared for overpasses between 6 and 25 August 2015, in the study region off the Western African coast between 40°N and 10°S latitude and 40°W and 40°E longitude, for a total of 45 overpasses. The four most significant cases are discussed here. For each overpass, the CATS aerosol extinction coefficient was compared with the MetUM dust extinction coefficient, and the modelled contribution to extinction of each of the two size bins was also analysed.

In fig 16, a CATS overpass at 00 UTC on the 7th August over the African continent is shown, with significant amounts of dust between 1 and 7 km. The MetUM predicts the dust in more or less the right places across the CATS track, but underpredicts the magnitude of the extinction coefficient. As for the case studies in the section 4.1, most of the predicted dust is also lower in altitude than in the observations (below 5km) than observed and extends to the surface (although the model does predict some dust reaching as high as 7 km). The smaller size bin contributes most to the modelled extinction coefficient.

In fig 17, a CATS overpass from 18 UTC also on the 7th August is shown, where the dust is moving off from the West African coast over the sea. At the Eastern end of the transect the model has a similar dust extinction coefficient to CATS, the key difference being that the model layer extends to the surface, while in the CATS observations it is elevated. However, over the ocean (longitude > 15°W) the model misses the layer evident in the CATS data.

Two further examples shown in fig 18 for 00 UTC on the 8th August and fig 19 for 16 UTC on the 10th August, showing a similar pattern. In fig 18 the entire CATS overpass shown is over land, and whilst there is reasonable agreement about the general location of the plume between the model prediction and the observations, the model has the dust extending to the surface with the bulk of the extinction too low in the atmosphere. It also under-predicts the amount of dust extinction significantly. In fig 19, the CATS overpass again starts over the West African coast and then moves over the ocean. As in the previous example, the model predicts a deep dust layer extending up to 6km. The model does predict some dust over the ocean, but beyond 15°W the aerosol extinction is again underestimated, with no dust in division d2 over ocean.

Two things stand out from the above examples: (1) over the African continent, where the dust is uplifted, the model generally agrees better with the observations than over the ocean further away from the source region, and (2) the smaller dust particles (division d1) in the model reach the same altitude as the dust layer observed by CATS, but the coarser particles (division d2) appear to be distributed much lower in the atmosphere (e.g Fig 16, 18 and 19). As already mentioned, we looked at similar plots for 45 overpasses in total, and the comparison gave similar results.

In the MetUM there is a size dependence in the dust uplift scheme, where finer particles are lofted more easily. However, previous studies suggest that the MetUM division d2 dust would be expected to reach higher altitudes away from source regions than it does. The behaviour downstream from the source seems to indicate that as the

https://doi.org/10.5194/acp-2020-57
Preprint. Discussion started: 16 April 2020


Atmospheric Chemistry and Physics Discussions

460 dust-laden air mass moves away, the coarse particles are lost too quickly in the model prediction. This would fit with what previous studies have found, for example Ansmann et al., (2017).

4.4. Effect of large scale wind and boundary layer height

In this section we investigate potential drivers for the observed discrepancies in the vertical distribution of dust in the MetUM and ECMWF CAMS. This is a difficult task as there are many competing factors that influence how
465 dust is lifted into the atmosphere and subsequently transported, and these vary considerably between models. In the MetUM the three processes which are most likely to have an impact on the vertical distribution of dust are the convection scheme, boundary layer (BL) height at source, and the largescale wind. Looking at the largescale wind field and BL height should show whether the modelled dust layer height is controlled by the largescale wind or by boundary layer mixing processes at the source. If examination of these processes cannot explain why the
470 dust is too low in altitude, then the most likely cause is to be researched in the convection scheme. There is, however, no direct measure of convection in the model output fields from the MetUM, and therefore any influence can only be inferred from the data that is available to us.

Backtrajectories from HYSPLIT and NAME and SEVIRI dust RGB imagery were used to determine the central trajectory of the dust sampled during each case study from source (Fig 1). The dust concentration for each size
475 bin, the large-scale wind (w) and the BL height were extracted from the model output along the track, and plotted as a cross-section every 6 hours from the time of uplift to the time of sampling by the aircraft.

Fig 20 displays such cross-sections for case study 3. The dust was uplifted from Mali on the 13th August, with a secondary uplift along the track, in Mauritania. At the time of uplift both models show an increase in the largescale wind velocity. This was observed for all the cases looked at. At the time of dust uplift, the BL height
480 was typically 4 – 5 km, and the dust mixed up to its top. The altitude to which the dust reached over the source regions of Africa compared well with the CATS observations of the depth of the dust layer over Africa (fig 16 - 19). This suggests that problems with the BL height in the MetUM may not be the cause for the dust layer being represented too low in the atmosphere away from the source region.

From the data presented here it is not possible to determine how well the models represent largescale wind in the
485 dust source regions. Previous studies which have looked at this issue more comprehensively do however suggest that there is an underprediction of wind fields in the models, which is also linked to coarse resolution modelling (eg. Chouza et al., 2016). Evan et al, (2016) showed that desert dust emission is to first order a function of wind speed, and it is against this quantity that models parametrise the dust source. Therefore, it seems reasonable that improving the wind speed in the models is a key part of getting the amount of dust uplift right.

490

5 Conclusions

The vertical distribution, particle size distribution, and mass concentration are the key properties that are predicted in a dust transport model. On the other hand, the main observable quantity on a global scale is

https://doi.org/10.5194/acp-2020-57
Preprint. Discussion started: 16 April 2020


Atmospheric Chemistry and Physics Discussions

aerosol optical depth, from AERONET (Holben et al., 1998), MODIS (Hsu et al, 2004, 2006, 2013; Levy et al, 2013; Sayer et al, 2013, 2014), and potentially other sources such as PMAP (Lang et al, 2017), VIIRS (Hsu et al, 2019), and several others. Aerosol optical depth is at the same time an optical property and a vertically integrated quantity, meaning that a same observable AOD can be retrieved e.g. with differing combinations of concentration and particle size distribution, or with a differing vertical distribution. It is good practice to pull the model towards the observations, and this can be achieved through tuning and through data assimilation: this means that we can expect a good model to yield a sensible prediction of the AOD. This is however insufficient to state that the underlying microphysical properties, from which AOD is derived, are correctly balanced.

The vertical distribution and particle size distribution heavily affect how dust is transported and how quickly it is deposited. Wind speed and direction are altitude dependent, meaning that transport is heavily dependent on the altitude of a layer. Residence time and transport range are affected by both the particle size distribution (coarse particles tend to be deposited more quickly) and vertical distribution (turbulent mixing in the boundary layer speeds up deposition, compared to the free troposphere). The representation of these properties in a model can affect the predicted AOD gradient across the Atlantic, for example. All this means that in the case of a model constrained by AOD observations only, other processes may need to compensate for a potential imbalance in the microphysical representation, such as e.g. the intensity of sources and sinks. The microphysical properties and the three-dimensional spatial distribution of dust are thus deeply interconnected.

We have used a combination of remote sensing and in-situ measurements to characterize the vertical distribution and transport of Saharan dust over the Eastern Atlantic and West Africa during August 2015, and to evaluate the dust forecasts from two operational global atmospheric models (MetUM and ECMWF CAMS). The dust AOD predictions at short forecast lead times from both models were in agreement with the aircraft, satellite, and AERONET observations, but with a low bias (note that both models assimilate AOD). On the other hand, we found that the vertical distribution of aerosol extinction coefficient and dust concentration could benefit from improvements. Our results show that the predicted vertical distribution places the dust low in the atmosphere, when compared to observations. Agreement between measured and modelled profiles was better near source, with differences increasing downstream. These results are in agreement with previous studies (e.g Kim et al., 2014, Ansmann et al., 2017).

This issue was particularly noticeable in the MetUM, where the coarser dust was not transported high enough in the atmosphere, or far enough away from source, compared with the observations. This suggests that the model could be settling the coarse mode dust too quickly, and similar findings have also been observed in previous studies (e.g Kim et al., 2014; Mona et al., 2014; Binietoglou et al., 2015). We also found that both models underpredict the coarse mode, and overpredict the fine mode. The discrepancy between the magnitude of the measured and modelled extinction coefficient is much less than for the concentration profiles. This is likely to be due to the microphysical representation, since small particles are more optically efficient. Due to MODIS AOD data assimilation, and model tuning against AERONET

https://doi.org/10.5194/acp-2020-57
Preprint. Discussion started: 16 April 2020


Atmospheric Chemistry and Physics Discussions

observations, the large under prediction of coarse mode dust in the models is compensated with a relatively small effect on the forecast average extinction coefficient and aerosol optical depth, even with the discrepancies in size distribution and dust concentration.

The overestimation of dust concentration in the finer ECMWF CAMS bins, and the underestimate of coarser dust is something that ECMWF are aiming to address in the future. In order to do this an updated dust emission scheme based on Remy et al (2019) using the Kok et al., (2012) estimates of size distribution at emission would be used. It is expected that this would increase the total dust concentration and shift it to the larger sizes, thus keeping total extinction similar to its present values, but more accurately representing the dust size distribution. After these changes have been implemented, a further study like the present one can help quantify the improvement introduced.

We have also investigated the processes driving dust uplift in the models, and our analysis suggests that uncertainties in the large-scale wind and the emitted size distribution are likely causes of differences between observations of the Saharan Air Layer (SAL) and MetUM predictions. The crude representation of the dust size-distribution in the MetUM 2-bin dust scheme is another important factor. The MetUM operational dust forecast is intended to be used primarily for AOD forecasts and extinction for visibility purposes, and although improvements of the microphysical properties would be desirable, the current implementation is satisfactory to an extent, and has the advantage of being computationally cheap. We also note that the dust scheme used in the Met Office climate model differs, using 6 size bins rather than 2, with the 6-bin version yet to be evaluated as in this article.

The scheme used to represent dust microphysical properties in models deserves attention as a key element to pursue accurate mineral dust predictions. Simple schemes (such as for instance the 2-bin dust size-distribution in the operational version of the MetUM) have the obvious advantage of being viable in terms of computing resources required, but on the other hand there is the consequence of giving a less accurate representation of the microphysical properties. This could be addressed by increasing the number of variables used to represent the size distribution, for example by using a scheme with 2 or more modes, each defined by 2 variables, such as in the GLOMAP-mode aerosol scheme in UKCA (Mulcahy et al, 2020), although the ability of this scheme to represent the coarse and giant modes correctly still needs to be proven. Whatever approach is chosen, it needs to allow for coarse and giant particles to be represented, a capability currently missing in many models (Huneeus et al, 2011). It is to be noted that there are plans in place to move to GLOMAP dust within the operational Global MetUM in the near future, and also ongoing experimentation with this scheme in the ECMWF IFS within CAMS. Moreover, there are plans to modify the latter scheme by adding a third (super coarse) mode: these are changes in the right direction.

As the size-distribution affects gravitational settling, it indirectly affects the three-dimensional distribution. Additionally, some processes may deserve better attention, as studies suggest that they could increase the lifetime of coarse and giant particles beyond what is predicted for gravitational settling: e.g. turbulence within the Saharan Air Layer, particle electrification, and the role of convective systems (Van Der Does et al, 2018). The optimum balance between these processes is still to be understood, as is the correct

https://doi.org/10.5194/acp-2020-57
Preprint. Discussion started: 16 April 2020


Atmospheric Chemistry and Physics Discussions

estimation of emission intensity. The dust observable properties, in terms of the aerosol optical depth, the particle sizes, the spatial distribution, and the vertical distribution, are determined by these processes. The combination of all these properties determines the impact of dust on the climate system, hence the importance of understanding these processes better (see e.g. Kok et al, 2017).

As this study highlights the limitations ascribed to using AOD as the main observable quantity towards which to verify, tune and pull the model, it also supports the perspective of improving the set of aerosol observations that can be used on a global scale. In particular, observational datasets exist for the vertical dust distribution, which can be exploited to better constrain the predictions. The most obvious one is the CALIPSO dataset, which has been observing the global aerosol distribution since 2006 (Winker et al, 2010; Liu et al, 2008; Tsamalis et al, 2013), and in the future EarthCARE is expected to be another very good candidate (Illingworth et al, 2015). Note that this perspective is not limited to using active sensors, and studies exist on the observation of the vertically resolved distribution from passive hyperspectral instruments in the infrared (Callewaert et al, 2019). In the long-term, providing observations not only of AOD, but also on the vertical distribution of aerosols, could become the driver for operational space missions.

In addition to vertically-resolved information, we also highlight the importance and need for better constrained size-resolved properties of dust, needed to reproduce the correct relationship between concentration and extinction coefficient. Particle size-distributions, both in the model representation and in the observations, should cover the whole size spectrum, including the giant mode (Marenco et al, 2018; Ryder et al, 2019). Ideally, these observations should be coordinated, vertically resolved, and established across a number of locations downstream from sources, e.g. across the Tropical Atlantic. Sporadic observations do exist, we are here advocating a more systematic approach. For instance, a number of balloonborne sensors are being developed and could be used for this purpose (see e.g. Renard et al, 2016; Fujiwara et al, 2016; Smith et al, 2019).

To conclude, we highlight how campaigns focusing on a combination of in-situ and remote sensing observations can provide information to at the same time validate existing model developments and help identify the areas requiring developments. In the last few years, considerable improvements have been made to operational dust forecasts, and with this paper we want to contribute to this effort by (1) indicating a few points that could be addressed in the models, and (2) provide a few datasets and a selection of case studies for future model assessments.

6 Acknowledgements

Airborne data were obtained using the BAe-146-301 Atmospheric Research Aircraft operated by Directflight Ltd and managed by the Facility for Airborne Atmospheric Measurements (FAAM).

The staff of the Met Office, the Universities of Leeds, Manchester and Hertfordshire, FAAM, Direct Flight, Avalon Engineering and BAE Systems are thanked for their dedication in making the ICE-D and AER-D campaigns a success. Claire Ryder acknowledges NERC support through Independent Research Fellowship NE/M018288/1. The authors thank the

https://doi.org/10.5194/acp-2020-57
Preprint. Discussion started: 16 April 2020

principal investigators and their staff for establishing and maintaining the AERONET sites used in this study. The MODIS data in this study were acquired as part of NASA's Earth Science Enterprise. The algorithms were developed by the MODIS Science Teams and the data were processed by the MODIS Adaptive Processing System (MODAPS) and Goddard Distributed Archive Centre (DAAC) and are archived and distributed by the Goddard DAAC. The authors gratefully acknowledge the NOAA Air Resources Laboratory for the provision of the HYSPLIT transport and dispersion model used in this publication.

The FAAM aircraft datasets collected during the ICE-D and AER-D campaigns are available from the British Atmospheric Data Centre, Centre for Environmental Data Analysis, at the following URL: http://catalogue.ceda.ac.uk/uuid/d7e02c75191a4515a28a208c8a069e70 (Bennett, 2019).

References

Ansmann, A., Petzold, A., Kandler, K., Tegen, I., Wendisch, M., Müller, D., Weinzierl, B., Müller, T., and Heintzenberg, J.: Saharan Mineral Dust Experiments SAMUM-1 and SAMUM-2: what have we learned?, Tellus, 63B, 403–429, 2011.

Ansmann, A., Rittmeister, F., Englemann, R., Basart, S., Benedetti, A., Spyrou, C., Skupin, A., Baars, H., Seifert, P., Senf, F., and Kanitz, T.: Profiling of Saharan dust from the Caribbean to West Africa, Part 2: Shipborne lidar measurements versus forecasts, Atmos. Chem. Phys. 2017

Benedetti, A., J.-J. Morcrette, O. Boucher, A. Dethof, R. J. Engelen, M. Fisher, H. Flentje, N. Huneeus, L. Jones, J. W. Kaiser, S. Kinne, A. Mangold, M. Razinger, A. J. Simmons, and M. Suttie.: Aerosol analysis and forecast in the European Centre for Medium-Range Weather Forecasts Integrated Forecast System: 2. Data assimilation. Journal of Geophysical Research, Atmospheres, 114, D13, doi:10.1029/2008JD011115, 2009

Bennett, L.: UK ICE-D: atmospheric measurements dataset collection, available at: http://catalogue.ceda.ac.uk/uuid/d7e02c75191a4515a28a208c8a069e70, last access: 10 December 2019.

Binietoglou, I., Basart, S., Alados-Arboledas, L., Amiridis, V., Argyrouli, A., Baars, H., Baldasano, J. M., Balis, D., Belegante, L., Bravo-Aranda, J. A., Burlizzi, P., Carrasco, V., Chaikovsky, A., Comerón, A., D'Amico, G., Filioglou, M., Granados-Muñoz, M. J., Guerrero-Rascado, J. L., Ilic, L., Kokkalis, P., Maurizi, A., Mona, L., Monti, F., Muñoz-Porcar, C., Nicolae, D., Papayannis, A., Pappalardo, G., Pejanovic, G., Pereira, S. N., Perrone, M. R., Pietruczuk, A., Posyniak, M., Rocadenbosch, F., Rodríguez-Gómez, A., Sicard, M., Siomos, N., Szkop, A., Terradellas, E., Tsekeri, A., Vukovic, A., Wandinger, U., and Wagner, J.: A methodology for investigating dust model performance using synergistic EARLINET/AERONET dust concentration retrievals, Atmos. Meas. Tech., 8, 3577–3600, https://doi.org/10.5194/amt-8-3577-2015, 2015.

Brooks M, D. Walters, B. Johnson (2011), Improvements to the size distribution of emitted dust in the South Asia Model, Technical Report DERTP/10/01-03, Met Office, Exeter, UK

https://doi.org/10.5194/acp-2020-57
Preprint. Discussion started: 16 April 2020

Callewaert, S., Vandenbussche, S., Kumps, N., Kylling, A., Shang, X., Komppula, M., Goloub, P., and De Mazière, M.: The Mineral Aerosol Profiling from Infrared Radiances (MAPIR) algorithm: version 4.1 description and evaluation, Atmos. Meas. Tech., 12, 3673–3698, https://doi.org/10.5194/amt-12-3673-2019, 2019.

Chouza, F., Reitebuch, O., Benedetti, A., and Weinzierl, B.: Saharan dust long-range transport across the Atlantic studied by an airborne Doppler wind lidar and the MACC model, Atmos. Chem. Phys., 16, 11581-11600, doi:10.5194/acp-16-11581-2016, 2016.

Cuevas, E., Camino, C., Benedetti, A., Basart< S., Terradellas, E., Baldasano, J.M., Morcrette, J.J., Marticorena, B., Goloub, P., Mortier, A., Berjón. A., Hernández, Y., Gil-Ojeda, M., and Schulz, M.: The MACC-II 2007-2008 reanalysis: atmospheric dust evaluation and characterization over northern Africa and the Middle East. Atmos. Chem. Phys., 15, 3991-4024, doi:10.5194/acp-15-3991-2015, 2015.

Collins, W., Bellouin, N., Doutriaux-Boucher, M., Gedney, N., Halloran, P., Hinton, T., Hughes, J., Jones, C., Joshi, M., Liddicoat, S., Martin, G., O'Connor, F., Rae, J., Senior, C., Sitch, S., Totterdell, I., Wiltshire, A., and Woodward, S. Development and evaluation of an Earth-System model – HadGEM2. Geosci. Model. Dev., 4, 1051-1075, doi:10.5194/gmd-4-1051-2011, 2011

Di Tomaso, E., Schutgens, N. A. J., Jorba, O., and Pérez García-Pando, C.: Assimilation of MODIS Dark Target and Deep Blue observations in the dust aerosol component of NMMB-MONARCH version 1.0, Geosci. Model Dev., 10, 1107–1129, https://doi.org/10.5194/gmd-10-1107-2017, 2017.

Draxler, R. R., and Hess, G.: An overview of the hysplit_4 modelling system for trajectories, Aust. Meteorol. Mag., 47, 295-308, 1998.

Evan, A.T., Surface Winds and Dust Biases in Climate Models, Geophysical Research Letters, 45, 2, 1079-1085, doi:10.1002/2017GL076353, 2018

Evan, A. T., Flamant, C., Gaetani, M., & Guichard, F. (2016). The past, present and future of African dust. Nature, 531(7595), 493–495.

Fujiwara, M., Sugidachi, T., Arai, T., Shimizu, K., Hayashi, M., Noma, Y., Kawagita, H., Sagara, K., Nakagawa, T., Okumura, S., Inai, Y., Shibata, T., Iwasaki, S., and Shimizu, A.: Development of a cloud particle sensor for radiosonde sounding, Atmos. Meas. Tech., 9, 5911–5931, https://doi.org/10.5194/amt-9-5911-2016, 2016.

Groß, S., Freudenthaler, V., Schepanski, K., Toledano, G., Schäfler, A., Ansmann, A., and Weinzierl, B.: Optical properties of long-range transported Saharan dust over Barbados as measured by dual-wavelength depolarization Raman lidar measurements. Atmos. Chem. Phys. 15, 11067-11080, doi:10.5194/acp-15-11067-2015, 2015

Heintzenberg, J.: The SAMUM-1 experiment over Southern Morocco: overview and introduction, Tellus, 61B, 2–11, 2009.

Holben, B.N., Eck, T.F., Slutsker, I., Tanré, D., Buis, J.P., Setzer, A., Vermote, E., Reagan, J.A., Kaufman, Y.J., Nakajima, T., Lavenu, F., Jankowiak, I., and Smirnov, A.: AERONET – a federated instrument network and data archive for aerosol characterization, Remote Sens. Environ., 66, 1-16, 1998.

Hsu, N.C. and Si-Chee Tsay and King, M.D. and Herman, J.R., Aerosol properties over bright-reflecting source regions, IEEE Transactions on Geoscience and Remote Sensing 42, 557-569, 2004, doi:10.1109/TGRS.2004.824067.

Hsu, N.C. and Si-Chee Tsay and King, M.D. and Herman, J.R., Deep Blue Retrievals of Asian Aerosol Properties During ACE-Asia, IEEE Transactions on Geoscience and Remote Sensing 44, 3180-3195, 2006, doi:10.1109/TGRS.2006.879540.

Hsu, N. C. and Jeong, M.-J. and Bettenhausen, C. and Sayer, A. M. and Hansell, R. and Seftor, C. S. and Huang, J. and Tsay, S.-C., Enhanced Deep Blue aerosol retrieval algorithm: The second generation, Journal of Geophysical Research Atmospheres 118, 9296-9315, 2013, doi:10.1002/jgrd.50712.

Hsu, N. C., Lee, J., Sayer, A. M., Kim, W., Bettenhausen, C., & Tsay, S.-C. (2019). VIIRS Deep Blue aerosol products over land: Extending the EOS long-term aerosol data records. Journal of Geophysical Research: Atmospheres, 124, 4026– 4053. https://doi.org/10.1029/2018JD029688

Huneeus, N., Schulz, M., Balkanski, Y., Griesfeller, J., Prospero, J., Kinne, S., Bauer, S., Boucher, O., Chin, M., Dentener, F., Diehl, T., Easter, R., Fillmore, D., Ghan, S., Ginoux, P., Grini, A., Horowitz, L., Koch, D., Krol, M. C., Landing, W., Liu, X., Mahowald, N., Miller, R., Morcrette, J.-J., Myhre, G., Penner, J., Perlwitz, J., Stier, P., Takemura, T., and Zender, C. S.: Global dust model intercomparison in AeroCom phase I, Atmos. Chem. Phys., 11, 7781–7816, https://doi.org/10.5194/acp-11-7781-2011, 2011.

Illingworth, A.J., H.W. Barker, A. Beljaars, M. Ceccaldi, H. Chepfer, N. Clerbaux, J. Cole, J. Delanoë, C. Domenech, D.P. Donovan, S. Fukuda, M. Hirakata, R.J. Hogan, A. Huenerbein, P. Kollias, T. Kubota, T. Nakajima, T.Y. Nakajima, T. Nishizawa, Y. Ohno, H. Okamoto, R. Oki, K. Sato, M. Satoh, M.W. Shephard, A. Velázquez-Blázquez, U. Wandinger, T. Wehr, G.-J. van Zadelhoff, 2015: The EarthCARE Satellite: The Next Step Forward in Global Measurements of Clouds, Aerosols, Precipitation, and Radiation, Bull. Am. Meteorol. Soc. 96, 1311-1332.

Johnson, B. T., B. Heese, S. A. McFarlane, P. Chazette, A. Jones, and N. Bellouin (2008), Vertical distribution and radiative effects of mineral dust and biomass burning aerosol over West Africa during DABEX, J. Geophys. Res., 113, D00C12, doi:10.1029/2008JD009848.

Jones A.R., Thomson D.J., Hort M. and Devenish B., 2007, The U.K. Met Office's next-generation atmospheric dispersion model, NAME III, Borrego C. and Norman A.-L. (Eds) Air Pollution Modeling and its Application XVII (Proceedings of the 27th NATO/CCMS International Technical Meeting on Air Pollution Modelling and its Application), Springer, pp. 580-589 https://doi.org/10.1007/978-0-387-68854-1_62.

Jickells, T., An, Z., Andersen, K. K., Baker, A., Bergametti, G., Brooks, N., Cao, J., Boyd, P., Duce, R., and Hunter, K.: Global iron connections between desert dust, ocean biogeochemistry, and climate, Science, 308, 67-71, 2005.

Karyampudi, V. M., Palm, S. P., Reagen, J. A., Fang, H., Grant, W. B., Hoff, R. M., Moulin, C., Pierce, H. F., Torres, O., Browell, E. V., and Melfi, S. H.: Validation of the Saharan dust plume conceptual model using lidar, Meteosat, and ECMWF data, B. Am. Meteorol. Soc., 80, 1045–1075, 1999.

Kanitz, T., Engelmann, R., Heinold, B., Baars, H., Skupin, A., and Ansmann, A.: Tracking the Saharan Air Layer with shipborne lidar acrossthe tropical Atlantic, Geophys. Res. Lett., 41, 1044–1050,2014.

Kim, D., Chin, M., Yu, H. B., Diehl, T., Tan, Q., Kahn, R. A., Tsigaridis, K., Bauer, S. E., Takemura, T., Pozzoli, L., Bellouin, N., Schulz, M., Peyridieu, S., Chedin, A., and Koffi, B.: Sources, sinks, and transatlantic transport of North African dust aerosol: A multimodel analysis and comparison with remote sensing data, J. Geophys. Res.-Atmos., 119, 6259–6277, https://doi.org/10.1002/2013jd021099, 2014.

Knippertz, P., and Todd, M. C.: Mineral dust aerosols over the sahara: Meteorological controls on emission and transport and implications for modeling, Rev. Geophys., 50, 2012.

Knollenberg, R. G.: Techniques for probing cloud microstructure, in: Clouds, Their Formation, Optical Properties, and Effects, edited by: Hobbs, P. V. and Deepak, A., 15–91, Academic Press, New York, USA, 1981.

Kok, J. F., Parteli, E. J., Michaels, T. I., & Karam, D. B. (2012). The physics of wind-blown sand and dust. Reports on Progress in Physics, 75(10), 106901.

Kok, J., Ridley, D., Zhou, Q. et al. Smaller desert dust cooling effect estimated from analysis of dust size and abundance. Nature Geosci 10, 274–278 (2017). https://doi.org/10.1038/ngeo2912

Lance, S., Brock, C. A., Rogers, D., and Gordon, J. A.: Water droplet calibration of the Cloud Droplet Probe (CDP) and in-flight performance in liquid, ice and mixed-phase clouds during ARCPAC, Atmos. Meas. Tech., 3, 1683–1706, https://doi.org/10.5194/amt-3-1683-2010, 2010.

Lang, R., A. Cacciari, A. Holdak, A. Kokhanovsky, M. Grzegorski, R. Munro, C. Retscher, R. Lindstrot, G. Poli, R. Huckle, N. Hao, S. Gimeno Garcia, PMAp Aerosol Optical Properties operational retrieval at global scale, presented at the EUMETSAT Meteorological Satellite Conference 2017, Rome, 2-6 October 2017.

Lavaysse, C., Chaboureau, J. P., and Flamant, C.: Dust impact on the west african heat low in summertime, 10 Q. J. Roy. Meteorol. Soc., 137, 1227-1240, 2011.

Levy, R. C. and Mattoo, S. and Munchak, L. A. and Remer, L. A. and Sayer, A. M. and Patadia, F. and Hsu, N. C., The Collection 6 MODIS aerosol products over land and ocean, Atmospheric Measurement Techniques 6, 2989-3034, 2013, doi:10.5194/amt-6-2989-2013.

Liu, P. S. K., Leaitch, W. R., Strapp, J. W., and Wasey, M. A.: Response of particle measuring systems airborne ASASP and PCASP to NaCl and latex particles, Aerosol Sci. Tech., 16, 83–95, 1992.

Liu, D., Z. Wang, Z. Liu, D. Winker, and C. Trepte (2008), A height resolved global view of dust aerosols from the first year CALIPSO lidar measurements, J. Geophys. Res.,113, D16214, doi:10.1029/2007JD009776.

Liu, Z., Q. Liu, H.-C. Lin, C. S. Schwartz, Y.-H. Lee, and T. Wang. Three-dimensional variational assimilation of MODIS aerosol optical depth: Implementation and application to a dust storm over East Asia. J. Geophys. Res., 116, D23206, doi:10.1029/2011JD016159. 2011

Liu, D., Taylor, J. W., Crosier, J., Marsden, N., Bower, K. N., Lloyd, G., Ryder, C. L., Brooke, J. K., Cotton, R., Marenco, F., Blyth, A., Cui, Z., Estelles, V., Gallagher, M., Coe, H., and Choularton, T. W.: Aircraft and ground measurements of dust aerosols over the west African coast in summer 2015 during ICE-D and AER-D, Atmos. Chem. Phys., 18, 3817–3838, https://doi.org/10.5194/acp-18-3817-2018, 2018.

Lopes, F. J. S., Landulfo, E., and Vaughan, M. A.: Evaluating CALIPSO's 532 nm lidar ratio selection algorithm using AERONET sun photometers in Brazil, Atmos. Meas. Tech., 6, 3281–3299, https://doi.org/10.5194/amt-6-3281-2013, 2013.

Marenco, F., Johnson, B., Turnbull, K., Newman, S., Haywood, J., Webster, H., and Ricketts, H. Airborne Lidar Observations of the 2010 Eyjafjallajökull volcanic ash plume. J. Geophys. Res. 116, D00U05, doi:10.1029/2011JD016396, 2011

Marenco, F. 2013. Nadir airborne lidar observations of deep aerosol layers. Atmos. Meas. Tech., 6, 2055-2064, doi:10.5194/amt-6-2055-2013, 2013

Marenco, F., Amiridis, V., Marinou, E., Tsekeri, A., and Pelon, J., Airborne verification of CALIPSO products over the Amazon: a case study of daytime observations in a complex atmospheric scene. Atmos. Chem. Phys., 14, 11871-11881, doi:10.5194/acp-14-11871-2014, 2014

Marenco, F., Johnson, B., Langridge, J., Mulcahy, J., Benedetti, A., Remy, S., Jones, L., Szpek, K., and Haywood, J. On the vertical distribution of smoke in the Amazonian atmosphere during the dry season. Atmos. Chem. Phys. 16, 2155-2174, doi:10.5194/acp-16-2155-2016, 2016.

Marenco, F., Ryder, C., Estellés, V., O'Sullivan, D., Brooke, J., Orgill, L., Lloyd, G. and Gallagher, M., Unexpected vertical structure of the Saharan Air Layer and giant dust particles during AER-D, Atmos. Chem. Phys. 18, 17655-17668, 2018.

Marsham, J. H., Hobby, M., Allen, C., Banks, J., Bart, M., Brooks, B., Cavazos-Guerra, C., Engelstaedter, S., Gascoyne, M., and Lima, A.: Meteorology and dust in the central sahara: Observations from fennec supersite-1 during the june 2011 intensive observation period, J. Geophys. Res. - Atmos., 118, 4069-4089, 2013.

McGill, M.J., Yorks, J.E., Scott, S.V., Kupchock, A.W., and Selmer, P.A. The Cloud-Aerosol Transport System (CATS): a technology demonstration on the International Space Station. Proc. SPIE 9612, Lidar Remote Sensing for Environmental Monitoring XV, 96120A . doi: 10.1117/12.2190841; https://doi.org/10.1117/12.2190841, 2015

Messager, C., Parker, D.J., Reitebuch, O., Agusti-Panareda, A., Taylor, C.M. and Cuesta, J. (2010), Structure and dynamics of the Saharan atmospheric boundary layer during the West African monsoon onset: observations and analyses from the research flights of 14 and 17 July 2006. Q.J.R. Meteorol. Soc., 136: 107-124. doi:10.1002/qj.469

Morcrette, J.-J., Boucher, O., Jones, L., Salmond, D., Bechtold, P., Beljaars, A., Benedetti, A., Bonet, A., Kaiser, J. W., Razinger, M., Schulz, M., Serrar, S., Simmons, A. J., Sofiev, M., Suttie, M., Tompkins, A. M., and Untch, A.: Aerosol analysis and forecast in the European Centre for Medium-Range Weather Forecasts Integrated Forecast System: Forward modeling, J. Geophys. Res., 114, D06206, https://doi.org/10.1029/2008JD011235, 2009.

Mona, L., Papagiannopoulos, N., Basart, S., Baldasano, J., Binietoglou, I., Cornacchia, C., and Pappalardo, G.: EARLINET dust observations vs. BSC-DREAM8b modeled profiles: 12-year-long systematic comparison at Potenza, Italy, Atmos. Chem. Phys., 14, 8781–8793, https://doi.org/10.5194/acp-14-8781-2014, 2014.

Mulcahy, J. P., D. N. Walters, N. Bellouin, and S. F. Milton. Impacts of increasing the aerosol complexity in the Met Office global numerical weather prediction model, Atmos. Chem. Phys., 14(9), 4749–4778, doi:10.5194/acp-14-4749-2014, 2014

Mulcahy, Jane P., Colin Johnson, Colin G. Jones, Adam C. Povey, Catherine E. Scott, Alistair Sellar, Steven T. Turnock, Matthew T. Woodhouse, N. Luke Abraham, Martin B. Andrews, Nicolas Bellouin, Jo Browse, Ken S. Carslaw, Mohit Dalvi, Gerd A. Folberth, Matthew Glover, Daniel Grosvenor, Catherine Hardacre, Richard Hill, Ben Johnson, Andy Jones, Zak Kipling, Graham Mann, James Mollard, Fiona M. O'Connor, Julien Palmieri, Carly Reddington, Steven T. Rumbold, Mark

Richardson, Nick A. J. Schutgens, Philip Stier, Marc Stringer, Yongming Tang, Jeremy Walton, Stephanie Woodward, and Andrew Yool, Description and evaluation of aerosol in UKESM1 and HadGEM3-GC3.1 CMIP6 historical simulations, submitted to Geoscientific Model Development (2020).

Niu, T., S. L. Gong, G. F. Zhu, H. L. Liu, X. Q. Hu, C. H. Zhou, and Y. Q. Wang. Data assimilation of dust aerosol observations for the CUACE/dust forecasting system. Atmos. Chem. Phys., 8(13), 3473–3482, doi:10.5194/acp-8-3473-2008. 2008

Osborne, S., Baran, A., Johnson, B., Haywood, J., Hesse, E., and Newman, S. (2008): Short-wave and long-wave radiative properties of saharan dust aerosol, Q. J. Roy. Meteorol. Soc., 137, 1149-1167, 2011.

Pope, R.J., Marsham, J.H., Knippertz, P., Brooks, M.E., and Roberts, A.J. Identifying errors in dust models from data assimilation. Geophysical Research Letters, 43, 9270-9279, doi:10.1002/2016GL070621, 2016

Rémy, S., Kipling, Z., Flemming, J., Boucher, O., Nabat, P., Michou, M., Bozzo, A., Ades, M., Huijnen, V., Benedetti, A., Engelen, R., Peuch, V.-H., and Morcrette, J.-J.: Description and evaluation of the tropospheric aerosol scheme in the European Centre for Medium-Range Weather Forecasts (ECMWF) Integrated Forecasting System (IFS-AER, cycle 45R1), Geosci. Model Dev., 12, 4627–4659, https://doi.org/10.5194/gmd-12-4627-2019, 2019.

Reddy, M. S., O. Boucher, N. Bellouin, M. Schulz, Y. Balkanski, J.-L.Dufresne, and M. Pham (2005), Estimates of global multicomponentaerosol optical depth and direct radiative perturbation in the Laboratoirede Me´te´orologie Dynamique General Circulation Model, J. Geophys.Res.,110, D10S16, doi:10.1029/2004JD004757.

Renard, J.-B., Dulac, F., Berthet, G., Lurton, T., Vignelles, D., Jégou, F., Tonnelier, T., Jeannot, M., Couté, B., Akiki, R., Verdier, N., Mallet, M., Gensdarmes, F., Charpentier, P., Mesmin, S., Duverger, V., Dupont, J.-C., Elias, T., Crenn, V., Sciare, J., Zieger, P., Salter, M., Roberts, T., Giacomoni, J., Gobbi, M., Hamonou, E., Olafsson, H., Dagsson-Waldhauserova, P., Camy-Peyret, C., Mazel, C., Décamps, T., Piringer, M., Surcin, J., and Daugeron, D.: LOAC: a small aerosol optical counter/sizer for ground-based and balloon measurements of the size distribution and nature of atmospheric particles – Part 1: Principle of measurements and instrument evaluation, Atmos. Meas. Tech., 9, 1721–1742, https://doi.org/10.5194/amt-9-1721-2016, 2016.

Ridley, D.A., Heald, C.L., Kok, J.F., and Zhao, C.: An observationally constrained estimate of global dust aerosol optical depth. Atmos. Chem. Phys., 16, 15097-15117, doi:10.5194/acp-16-15097-2016, 2016.

Richardson, M. S., DeMott, P. J., Kreidenweis, S. M., Cziczo, D. J., Dunlea, E. J., Jimenez, J. L., Thomson, D. S., Ashbaugh, L. L., Borys, R. D., and Westphal, D. L.: Measurements of heterogeneous ice nuclei in the western 5 united states in springtime and their relation to aerosol characteristics, J. Geophys. Res. - Atmos., 112, 2007

Roberts, A. J., Woodage, M. J., Marsham, J. H., Highwood, E. J., Ryder, C. L., McGinty, W., Wilson, S., and Crook, J.: Can explicit convection improve modelled dust in summertime West Africa?, Atmos. Chem. Phys., 18, 9025–9048, https://doi.org/10.5194/acp-18-9025-2018, 2018.

Ryder, C., McQuaid, J., Flamant, C., Rosenberg, P., Washington, R., Brindley, H., Highwood, E., Marsham, J., Parker, D., Todd, M., Banks, J., Brooke, J., Engelstaedter, S., Estelles, V., Formenti, P., Garcia-Carreras, L., Kocha, C., Marenco, F., Sodemann, H., Allen, C., Bourdon, A., Cavazos-Guerra, M., Chevaillier, S., Crosier, J., Derbyshire, E., Dean, A., Dorsey, J., Kent, J., O'Sullivan, D., Schepanski, K., Szpek, K., Trembath, J., and Woolley A.: Advances in understanding mineral dust

and boundary layer processes over the Sahara from Fennec aircraft observations. Atmos. Chem, Phys., 15, 8479-8520, doi:10.5194/acp-15-8479-2015, 2015

Ryder, C.L., F. Marenco, J.K. Brooke, V. Estelles, R. Cotton, P. Formenti, J.B. McQuaid, H.C. Price, D. Liu, P. Ausset, P.D. Rosenberg, J.W. Taylor, T. Choularton, K. Bower, H. Coe, M. Gallagher, J. Crosier, G. Lloyd, E.J. Highwood, and B.J. Murray, Coarse-mode mineral dust size distributions, composition and optical properties from AER-D aircraft measurements over the tropical eastern Atlantic, Atmos. Chem. Phys. 18, 17225-17257, 2018.

Ryder, C. L., Highwood, E. J., Walser, A., Seibert, P., Philipp, A., and Weinzierl, B.: Coarse and giant particles are ubiquitous in Saharan dust export regions and are radiatively significant over the Sahara, Atmos. Chem. Phys., 19, 15353–15376, https://doi.org/10.5194/acp-19-15353-2019, 2019.

Sayer, A. M. and Hsu, N. C. and Bettenhausen, C. and Jeong, M.-J., Validation and uncertainty estimates for MODIS Collection 6 "Deep Blue" aerosol data, Journal of Geophysical Research Atmospheres 118, 7864-7872, 2013, doi:10.1002/jgrd.50600.

Sayer, A. M. and Munchak, L. A. and Hsu, N. C. and Levy, R. C. and Bettenhausen, C. and Jeong, M.-J., MODIS Collection 6 aerosol products: Comparison between Aqua's e-Deep Blue, Dark Target, and "merged" data sets, and usage recommendations, J. Geophys. Res. Atmos. 119, 13,965-13,989, 2014, doi:10.1002/2014jd022453.

Scanza, R.A., Mahowald, N., Ghan, S., Zender, C.S., Kok, J.F., Liu, X., Zhang, Y., and Albani, S.: Modeling dust as component minerals in the Community Atmosphere Model: development of framework and impact on radiative forcing. Atmos. Chem. Phys., 15, 537-561, doi:10.5194/acp-15-537-2015, 2015.

Schepanski, K., Tegen, I., Laurent, B., Heinold, B., and Macke, A.: A new saharan dust source activation frequency map derived from msg-seviri ir-channels, Geophys. Res. Lett., 34, 2007.

Smith, H. R., Ulanowski, Z., Kaye, P. H., Hirst, E., Stanley, W., Kaye, R., Wieser, A., Stopford, C., Kezoudi, M., Girdwood, J., Greenaway, R., and Mackenzie, R.: The Universal Cloud and Aerosol Sounding System (UCASS): a low-cost miniature optical particle counter for use in dropsonde or balloon-borne sounding systems, Atmos. Meas. Tech., 12, 6579–6599, https://doi.org/10.5194/amt-12-6579-2019, 2019.

Sodemann, H., Lai, T., Marenco, F., Ryder, C. L., Flamant, C., Knippertz, P., Rosenberg, P., Bart, M., and Mcquaid, J. B.: Lagrangian dust model simulations for a case of moist convective dust emission and transport in the western sahara region during fennec/ladunex, J. Geophys. Res. - Atmos., 120, 6117-6144, 2015.

Stein, A.F., Draxler, R.R, Rolph, G.D., Stunder, B.J.B., Cohen, M.D., and Ngan, F., (2015). NOAA's HYSPLIT atmospheric transport and dispersion modeling system, Bull. Amer. Meteor. Soc., 96, 2059-2077, http://dx.doi.org/10.1175/BAMS-D-14-00110.1

Tsamalis, C., Chédin, A., Pelon, J., and Capelle, V.: The seasonal vertical distribution of the saharan air layer and its modulation by the wind, Atmos. Chem. Phys., 13, 11235-11257, 2013.

Walters, D., I. Boutle, M. Brooks, T. Melvin, R. Stratton, S. Vosper, H. Wells, K. Williams, N. Wood, T. Allen, A. Bushell, D. Copsey, P. Earnshaw, J. Edwards, M. Gross, S. Hardiman, C. Harris, J. Heming, N. Klingaman, R. Levine, J. Manners, G. Martin, S. Milton, M. Mittermaier, C. Morcrette, T. Riddick, M. Roberts, C. Sanchez, P. Selwood, A. Stirling, C. Smith, D.

https://doi.org/10.5194/acp-2020-57
Preprint. Discussion started: 16 April 2020

Atmospheric Chemistry and Physics Discussions

Suri, W. Tennant, P.L. Vidale, J. Wilkinson, M. Willett, S. Woolnough, and P. Xavier, "The Met Office Unified Model Global Atmosphere 6.0/6.1 and JULES Global Land 6.0/6.1 configurations", Geosci. Model Dev., 10, 1487-1520, doi:10.5194/gmd-10-1487-2017, 2017.

Winker, D.M., J. Pelon, J.A. Coakley, S.A. Ackerman, R.J. Charlson, P.R. Colarco, P. Flamant, Q. Fu, R.M. Hoff, C. Kittaka*, T.L. Kubar, H. Le Treut, M.P. McCormick, G. Mégie*, L. Poole, K. Powell, C. Trepte, M.A. Vaughan, and B.A. Wielicki, 2010: The CALIPSO Mission: A Global 3D View of Aerosols and Clouds, Bull. Am. Meteorol. Soc. 91, 1211-1228.

Woodward, S.: Modeling the atmospheric life cycle and radiative impact of mineral dust in the Hadley Centre climate model. J. Geophys. Res., 106, 18 155 – 18 166. Doi:10.1029/2000JD900795, 2001

Woodward, S.: Mineral Dust in HadGEM2, Hadley Centre Technical Note 87. Met Office Hadley Centre for Climate Change, Exeter, UK, http://www.metoffice.gov.uk/archive/science/climate-science/hctn87, 2011

Yorks, J.E., McGill, M.J., Palm, S.P., Hlavka, D.L., Selmer, P.A., Nowottnick, E., Vaughan, M.A., Rodier, S., and Hart, W.D.: An Overview of the CATS Level 1 Data Products and Processing Algorithms, Geophys. Res. Let., 43, doi:10.1002/2016GL068006 2016.

Van Der Does, Michèlle, Peter Knippertz, Philipp Zschenderlein, R. Giles Harrison, and Jan-Berend W. Stuut, The mysterious long-range transport of giant mineral dust particles, Sci. Adv. 4, doi: 10.1126/sciadv.aau2768, 2018.

https://doi.org/10.5194/acp-2020-57
Preprint. Discussion started: 16 April 2020

Atmospheric Chemistry and Physics Discussions

Flight	Flight section	Time	Lat N	Lon W	Aerosol extinction coefficient (Mm^{-1})			
					Data source	Mean	Stdev	Max
B920 7 Aug	R1	14:29:28 to 15:00:25	15.56 to 17.54	22.98 to 21.40	ECMWF	55	38	126
					MetUM	58	41	177
					Lidar	57	47	329
	R6	17:29:11 to 18:00:18	15.54 to 17.54	22.99 to 21.40	ECMWF	55	38	126
					MetUM	58	41	177
					Lidar	56	40	212
B923 12 Aug	R1	09:18:08 to 11:51:28	16.03 to 27.30	22.97 to 13.82	ECMWF	140	120	490
					MetUM	90	120	720
					Lidar	110	130	1130
B924 12 Aug	R3-R4	15:11:57 to 16:04:43	23.26 to 24.49	18.81 to 17.81	ECMWF	169	97	485
					MetUM	51	27	205
					Lidar	180	180	1260
	R6-R7	16:48:29 to 18:33:01	16.44 to 24.08	23.03 to 18.18	ECMWF	107	84	443
					MetUM	46	35	169
					Lidar	60	100	1150
B927 15 Aug	R1	13:59:06 to 14:46:00	11.42 to 15.05	24.55 to 23.37	ECMWF	81	60	332
					MetUM	54	41	159
					Lidar	78	96	372
B932 20 Aug	R1	09:52:41 to 10:35:23	17.72 to 20.67	21.19 to 18.93	ECMWF	140	120	500
					MetUM	140	130	620
					Lidar	76	81	395

Table 1: Summary of the high-level sections from each of the flights used here. Flight sections are labelled with the letter R (runs), see text. All times UTC.

865

https://doi.org/10.5194/acp-2020-57
Preprint. Discussion started: 16 April 2020

Atmospheric Chemistry and Physics Discussions

Flight	Flight section	Time	Lat N	Lon W	Altitude AMSL (km)
B920 7 Aug	P1	14:03:33 to 14:25:21	14.94 to 15.76	22.78 to 23.48	0.1 to 6.5
	P2	15:02:59 to 15:24:05	16.26 to 17.43	21.37 to 22.38	0.1 to 6.5
	P7	17:08:08 to 17:27:50	17.34 to 17.94	21.00 to 21.53	0.1 to 6.5
B923 12 Aug	P1	11:51:28 to 12:09:28	27.30 to 28.44	13.71 to 13.87	0.1 to 6.9
B932 20 Aug	P4	10:37:23 to 11:01:22	20.01 to 20.30	18.88 to 20.22	0.1 to 6.5

Table 2: Summary of the aircraft profiles from each of the flights used here. Flight sections are labelled with the letter P (profiles), see text. All times UTC.

https://doi.org/10.5194/acp-2020-57
Preprint. Discussion started: 16 April 2020

Atmospheric Chemistry and Physics Discussions

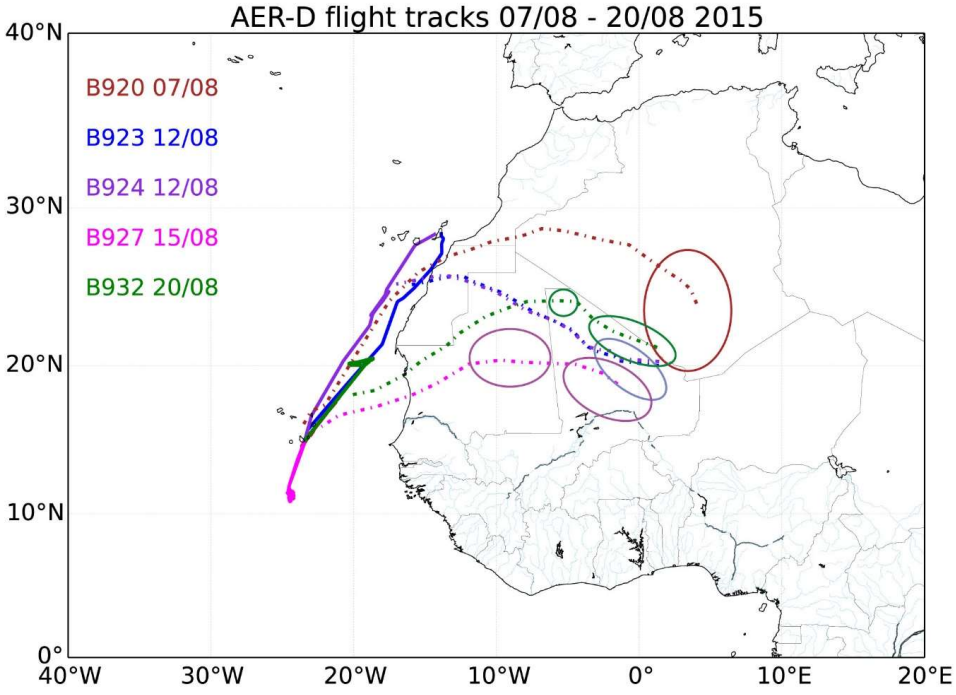

870 Figure 1. Flight tracks and dust source locations (circles). Dotted lines between flight tracks and circles show the approximate mean trajectory based on SEVIRI RGB dust images, NAME and HYSPLIT back trajectories. Note that flights B923/B924 sampled the same dust event.

https://doi.org/10.5194/acp-2020-57
Preprint. Discussion started: 16 April 2020

Atmospheric Chemistry and Physics Discussions

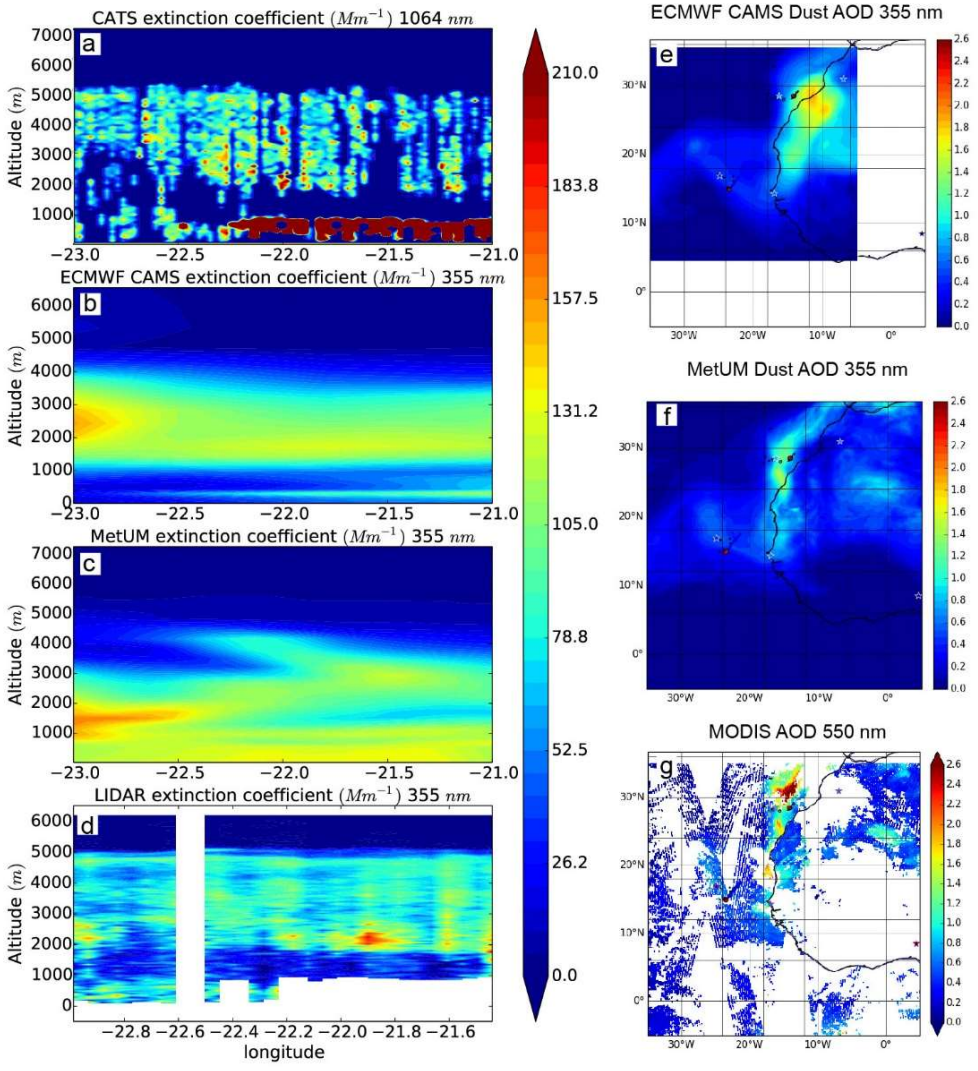

Figure 2: Case study 1, B920, 7th August, R6: (a-d) Vertical cross –section along the flight track showing the aerosol extinction coefficient for the CATS lidar (a), ECMWF CAMS (b), MetUM (c) and the aircraft lidar (d), the colour scale is the same for all four plots. (e) ECMWF AOD map, (f) MetUM AOD map and (g) AOD map from combined observations from MODIS, AERONET (stars) and aircraft lidar (dots).

https://doi.org/10.5194/acp-2020-57
Preprint. Discussion started: 16 April 2020

Atmospheric Chemistry and Physics Discussions

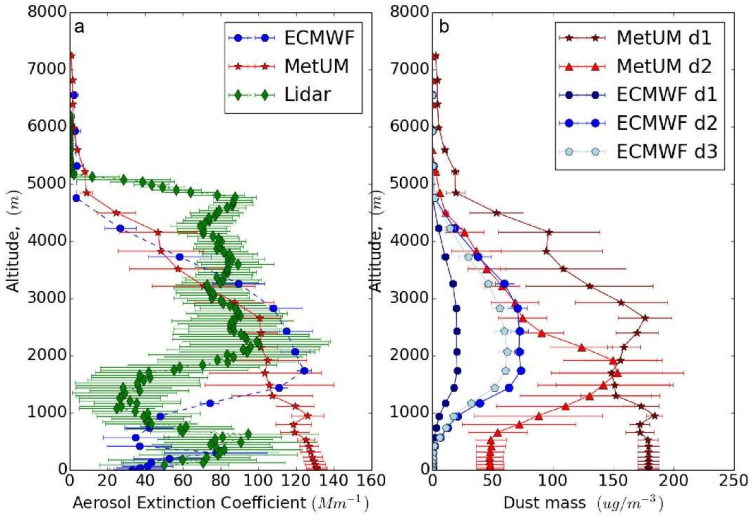

880 Figure 3: Case Study 1, B920, 7th August, R6; (a) Mean and standard deviation of the airborne lidar (green), MetUM (red) and ECMWF (blue) extinction profiles. (b) Modelled MetUM dust concentration for divisions 1 (dark red) and 2 (red), and modelled ECMWF concentration for divisions 1 (dark blue), 2 (blue) and 3 (light blue) dust concentration. See text for the description of the divisions.

885

https://doi.org/10.5194/acp-2020-57
Preprint. Discussion started: 16 April 2020

Atmospheric Chemistry and Physics Discussions

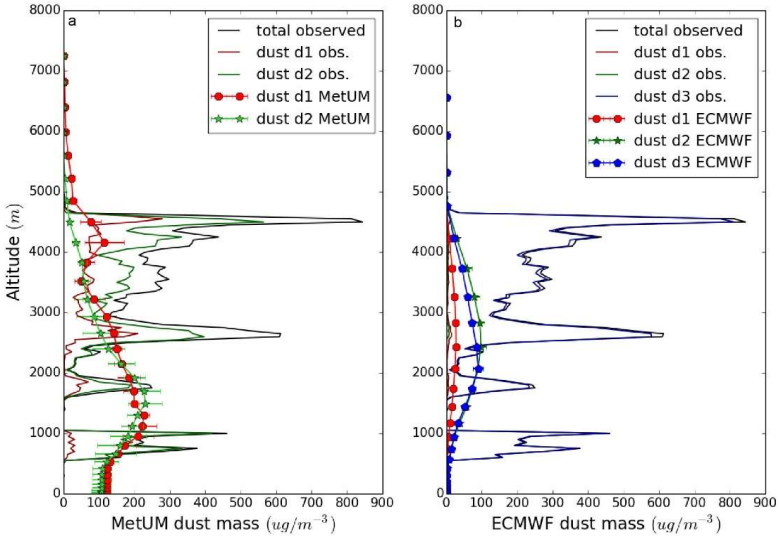

Figure 4: Case Study 1, B920, 7th August, P1. (a) Dust concentration measured by the in-situ instruments on the aircraft for MetUM dust divisions 1 (red) and 2 (green), and the total dust concentration measured (black). The division 1 and 2 concentration from the model is shown in a lighter shade of red and green respectively, with markers and error bars showing the standard deviation. (b) The right hand plot shows the same thing but for the ECMWF CAMS size bins, with the measurements shown using lines, and the model values with lines and markers for divisions 1 (red), 2 (green), and division 3 (blue). See text for the description of the divisions.

https://doi.org/10.5194/acp-2020-57
Preprint. Discussion started: 16 April 2020

Atmospheric Chemistry and Physics Discussions

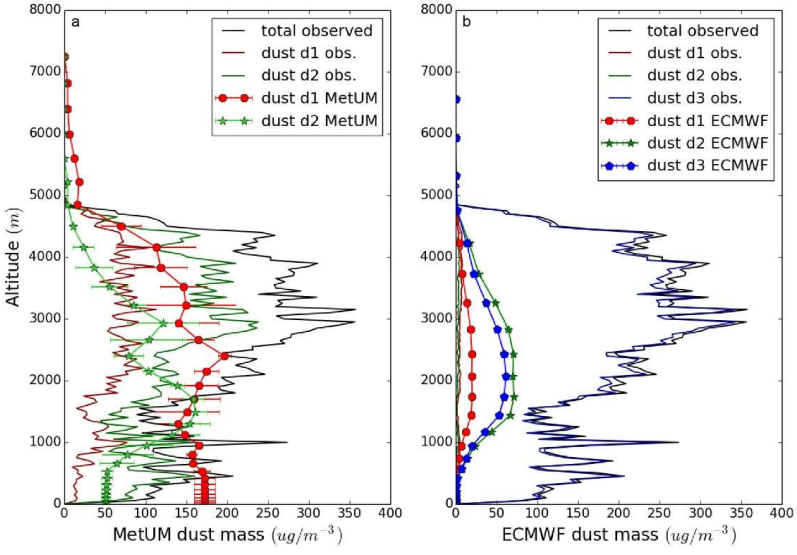

Figure 5: Case Study 1, B920, 7th August, P2. (a) Dust concentration measured by the in-situ instruments on the aircraft for MetUM dust divisions 1 (red) and 2 (green), and the total dust concentration measured (black). The division 1 and 2 concentration from the model is shown in a lighter shade of red and green respectively, with markers and error bars showing the standard deviation. (b) The right hand plot shows the same thing but for the ECMWF CAMS size bins, with the measurements shown using lines, and the model values with lines and markers for divisions 1 (red), 2 (green), and 3 (blue).

https://doi.org/10.5194/acp-2020-57
Preprint. Discussion started: 16 April 2020

Atmospheric Chemistry and Physics Discussions

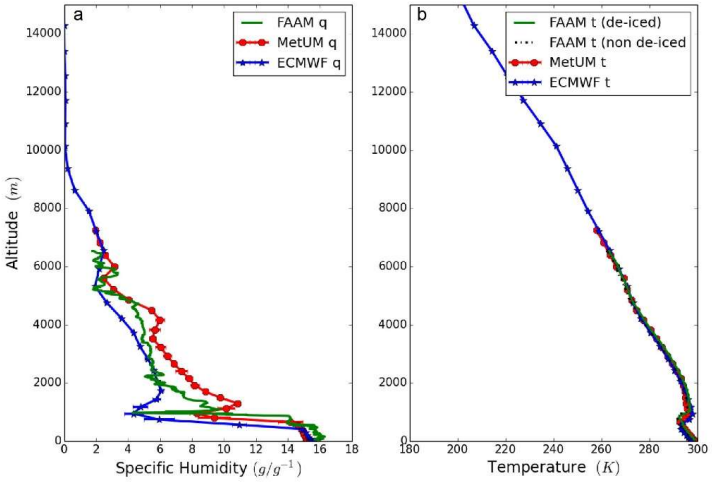

905 Figure 6: Case Study 1, B920, 7th August, P2. (a) water vapour mixing ratio from the aircraft measurements in the profile (green), compared with the MetUM (red) and ECMWF (blue). (b) the same but for temperature – here there are two measurements of temperature shown which are in good agreement.

https://doi.org/10.5194/acp-2020-57
Preprint. Discussion started: 16 April 2020

Atmospheric Chemistry and Physics Discussions

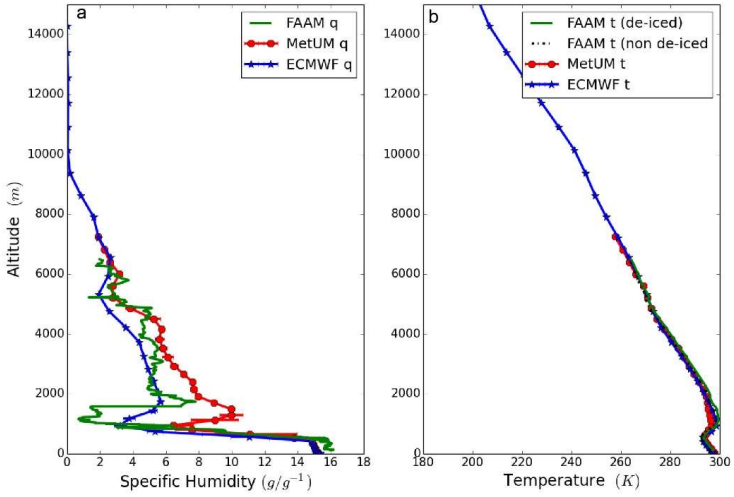

910

Figure 7: Case Study 1, B920, 7th August, P7. (a) water vapour mixing ratio from the aircraft measurements in the profile (green), compared with the MetUM (red) and ECMWF CAMS (blue). (b) the same but for temperature – here there are two measurements of temperature shown which are in good agreement.

https://doi.org/10.5194/acp-2020-57
Preprint. Discussion started: 16 April 2020

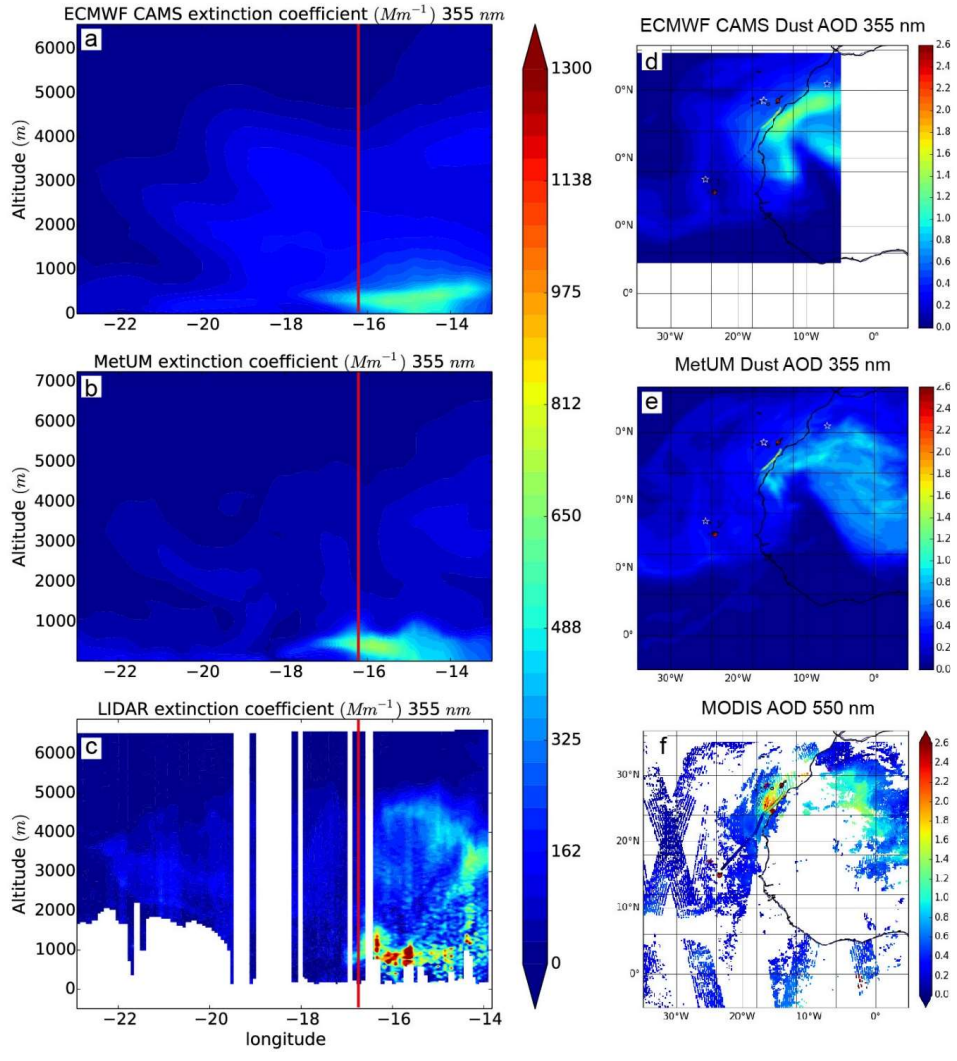

Figure 8: Case Study 2: B923, 12th August, R1: (a-c) Vertical cross –section along the flight track showing the aerosol extinction coefficient for ECMWF CAMS (a), MetUM (b) and the aircraft lidar (c), the colour scale is the same for all three plots. (d) ECMWF CAMS AOD map, (e) MetUM AOD map and (f) AOD map from combined observations from MODIS, AERONET (stars) and aircraft lidar (dots).

https://doi.org/10.5194/acp-2020-57
Preprint. Discussion started: 16 April 2020

Atmospheric Chemistry and Physics Discussions

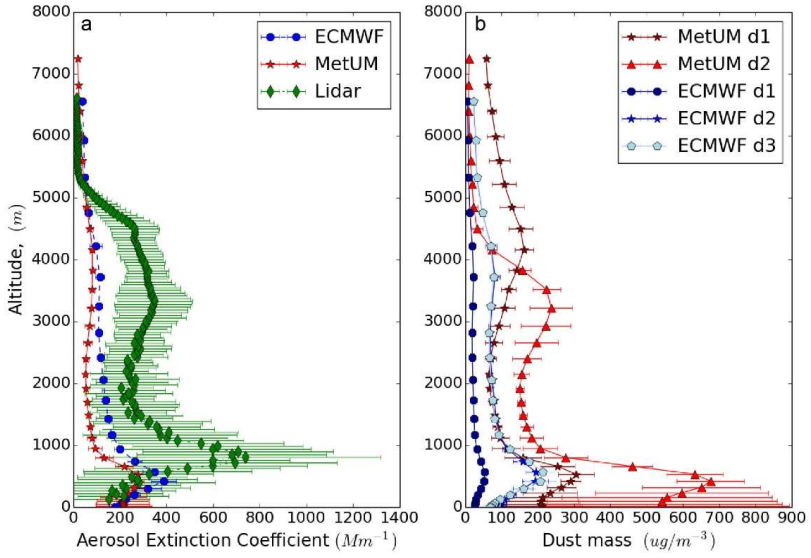

Figure 9: Case Study 2: B923, 12th August, R1: (a) Mean and standard deviation of the lidar (green), MetUM (red) and ECMWF (blue) extinction profiles. (b) Modelled MetUM dust concentration for divisions 1 (dark red) and 2 (red) and modelled ECMWF concentration for divisions 1 (dark blue), 2 (blue) and 3 (light blue) dust concentration.

https://doi.org/10.5194/acp-2020-57
Preprint. Discussion started: 16 April 2020

Atmospheric Chemistry and Physics Discussions

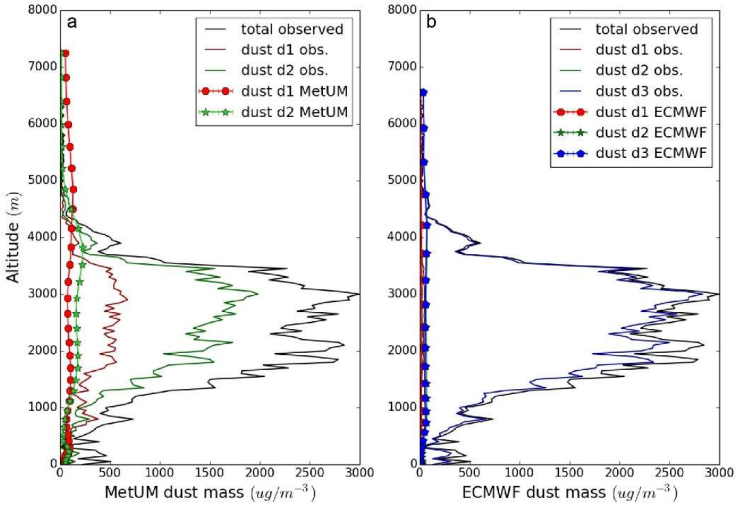

Figure 10: Case Study 2: B923, 12th August, P1 (landing in Fuerteventura). (a) Dust concentration measured by the in-situ instruments on the aircraft for two MetUM dust divisions 1 (red), and 2 (green), and the total dust concentration measured (black). The division 1 and 2 concentration from the model is shown in a lighter shade of red and green respectively, with markers and error bars showing the standard deviation. (b) The right-hand plot shows the same thing but for the ECMWF CAMS size bins, with the measurements shown using lines, and the model values with lines and markers for divisions 1 (red), 2 (green), and 3 (blue).

https://doi.org/10.5194/acp-2020-57
Preprint. Discussion started: 16 April 2020

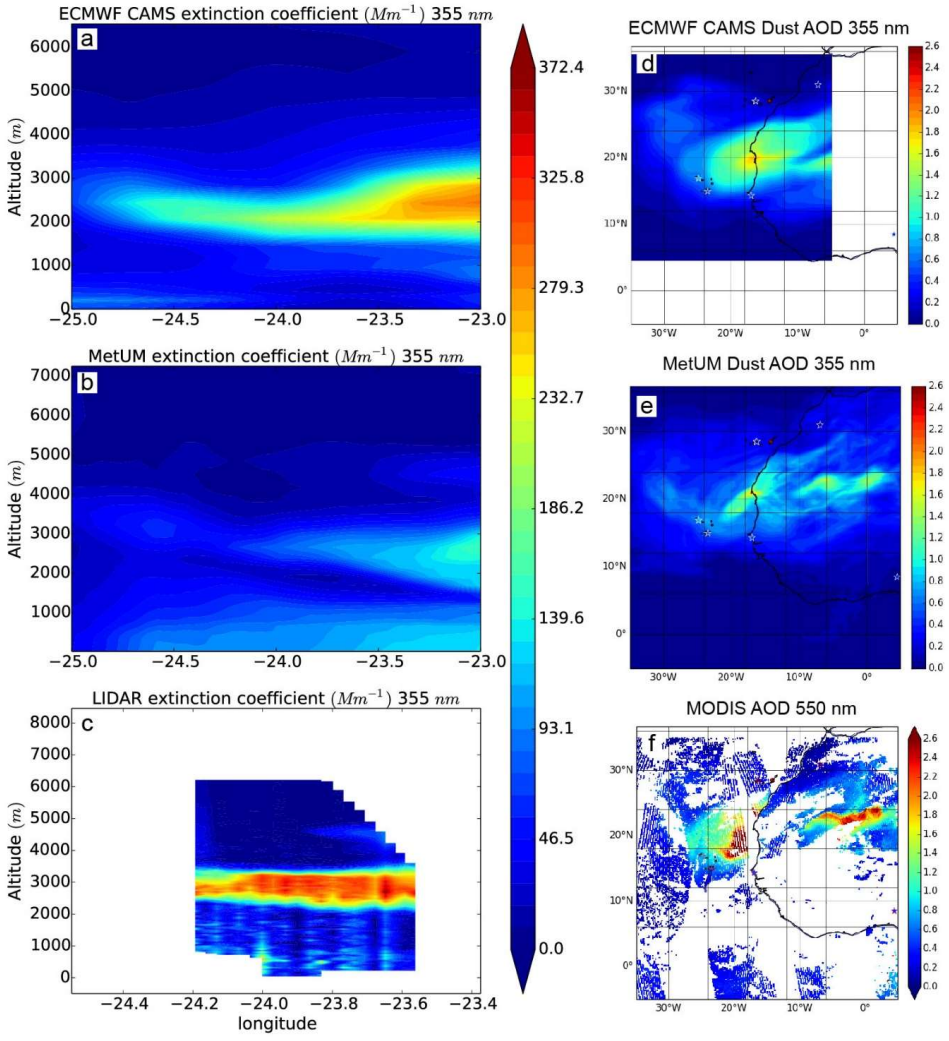

Figure 11: Case Study 3: B927, 15th August, R1: (a-c) Vertical cross –section along the flight track showing the aerosol extinction coefficient for ECMWF CAMS (a), MetUM (b) and the aircraft lidar (c), the colour scale is the same for these three plots. (d) ECMWF AOD map, (e) MetUM AOD map and (f) AOD map from combined observations from MODIS, AERONET (stars) and aircraft lidar (dots).

https://doi.org/10.5194/acp-2020-57
Preprint. Discussion started: 16 April 2020

Atmospheric Chemistry and Physics Discussions

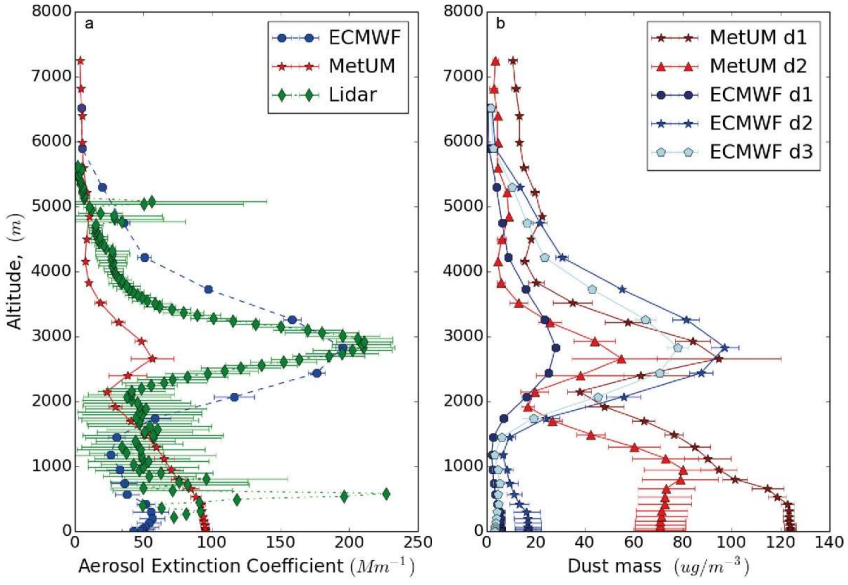

Figure 12: Case Study 3: B927, 15th August, R1: (a) Mean and standard deviation of the lidar (green), MetUM (red) and ECMWF (blue) extinction profiles. (b) Modelled MetUM dust concentration for divisions 1 (dark red) and 2 (red), and modelled ECMWF concentration for divisions 1 (dark blue), 2 (blue) and 3 (light blue) dust concentration.

https://doi.org/10.5194/acp-2020-57
Preprint. Discussion started: 16 April 2020

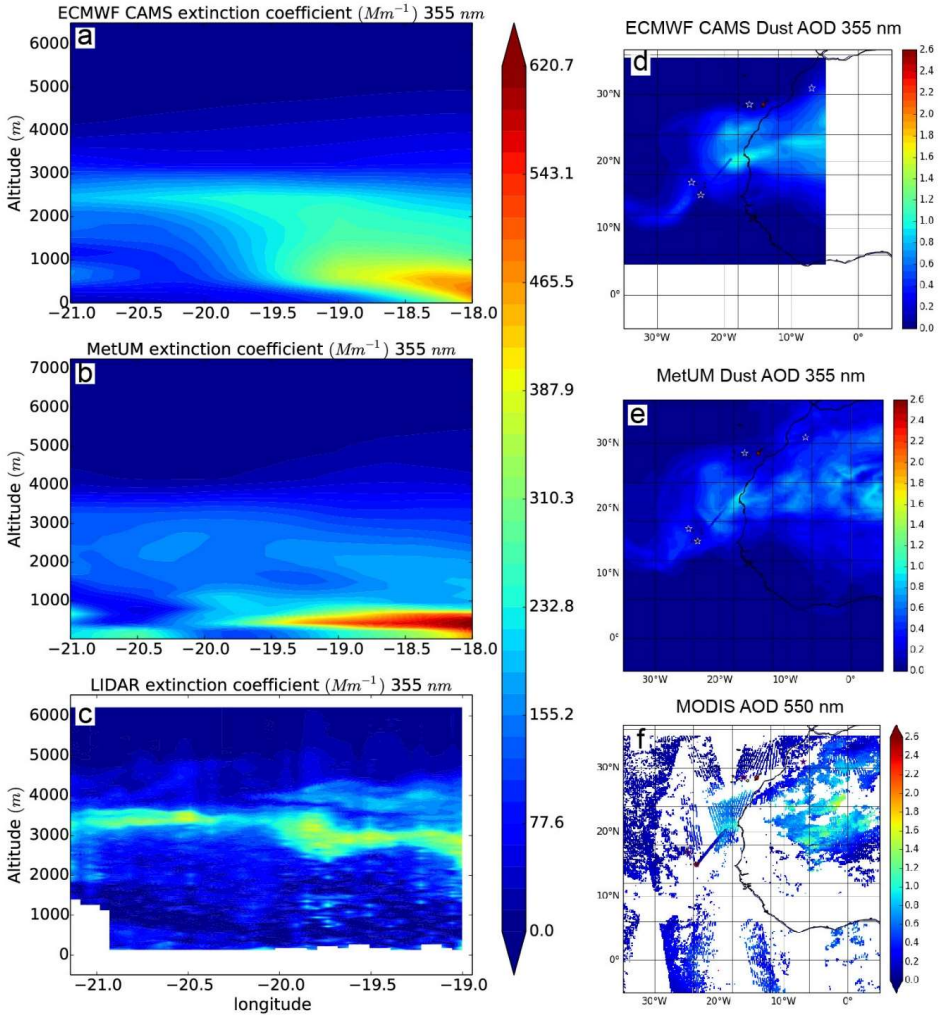

Figure 13: Case Study 4: B932, 20th August, R1: (a-c) Vertical cross –section along the flight track showing the aerosol extinction coefficient for ECMWF CAMS (a), MetUM (b) and the aircraft lidar (c), the colour scale is the same for all four plots. (d) ECMWF AOD map, (e) MetUM AOD map and (f) AOD map from combined observations from MODIS, AERONET (stars) and aircraft lidar (dots).

https://doi.org/10.5194/acp-2020-57
Preprint. Discussion started: 16 April 2020

Atmospheric Chemistry and Physics Discussions

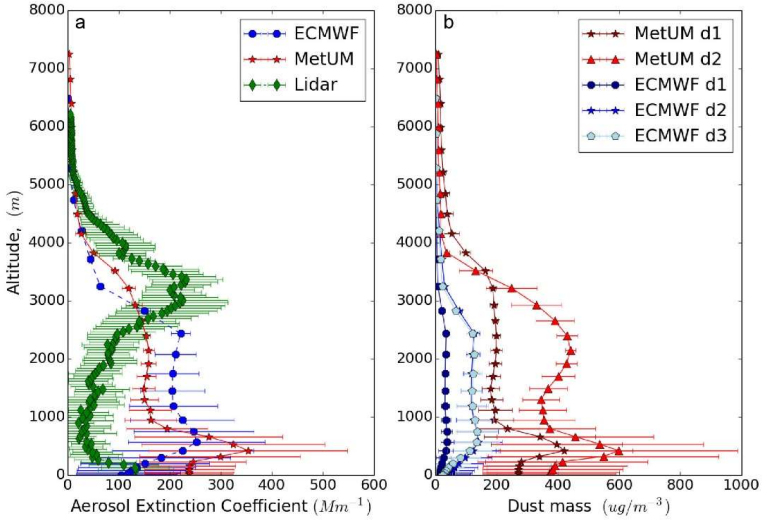

Figure 14: Case Study 4: B932, 20th August, R1: (a) Mean and standard deviation of the lidar (green), MetUM (red) and ECMWF (blue) extinction profiles. (b) Modelled MetUM concentration for divisions 1 (dark red), 2 (red), and modelled ECMWF concentration for divisions 1 (dark blue), 2 (blue) and 3 (light blue) dust concentration.

https://doi.org/10.5194/acp-2020-57
Preprint. Discussion started: 16 April 2020

Atmospheric Chemistry and Physics Discussions

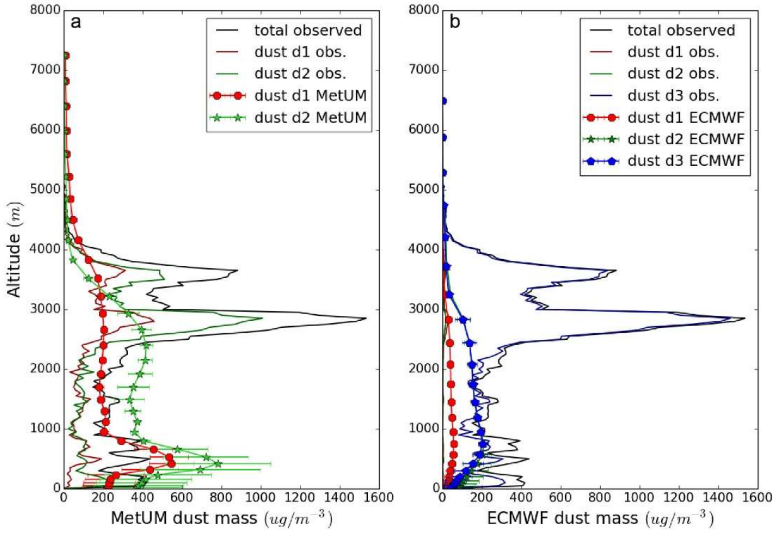

960 Figure 15: Case Study 4: B932, 20th August, P4. (a) Dust concentration measured by the in-situ instruments on the aircraft for two MetUM dust divisions 1 (red), and 2 (green), and the total dust concentration measured (black). The division 1 and 2 concentration from the model is shown in a lighter shade of red and green respectively, with markers and error bars showing the standard deviation. (b) The right hand plot shows the same thing but for the ECMWF CAMS size bins, with
965 the measurements shown using lines, and the model values with lines and markers for divisions 1 (red), 2, (green), and 3 (blue).

https://doi.org/10.5194/acp-2020-57
Preprint. Discussion started: 16 April 2020

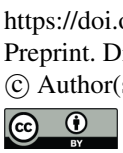

Atmospheric Chemistry and Physics Discussions

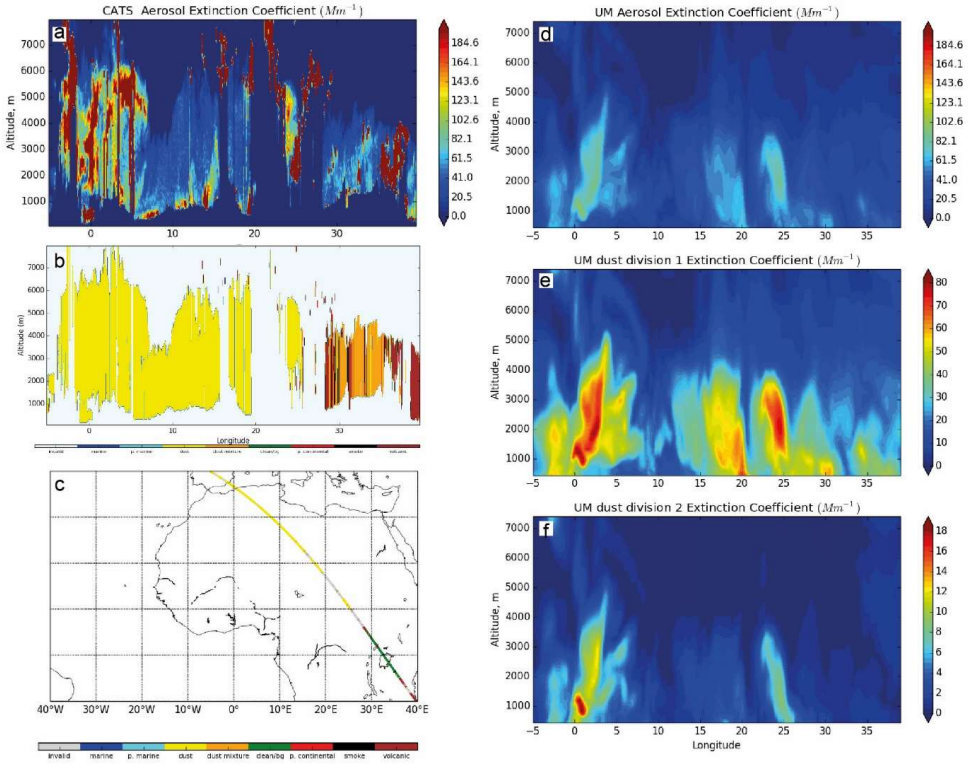

Figure 16: (a-c) CATS and (d-f) MetUM data for 00z on the 7th August, in the form of vertical cross–sections along the satellite track: (a) CATS extinction coefficient; (b) CATS feature type; (c) CATS overpass track; (d) MetUM total dust extinction coefficient; (e) MetUM d1 dust extinction coefficient; and (f) MetUM d2 dust extinction coefficient. Note that panel (a) may include some cloud signal (compare with panel b).

https://doi.org/10.5194/acp-2020-57
Preprint. Discussion started: 16 April 2020

Atmospheric Chemistry and Physics Discussions

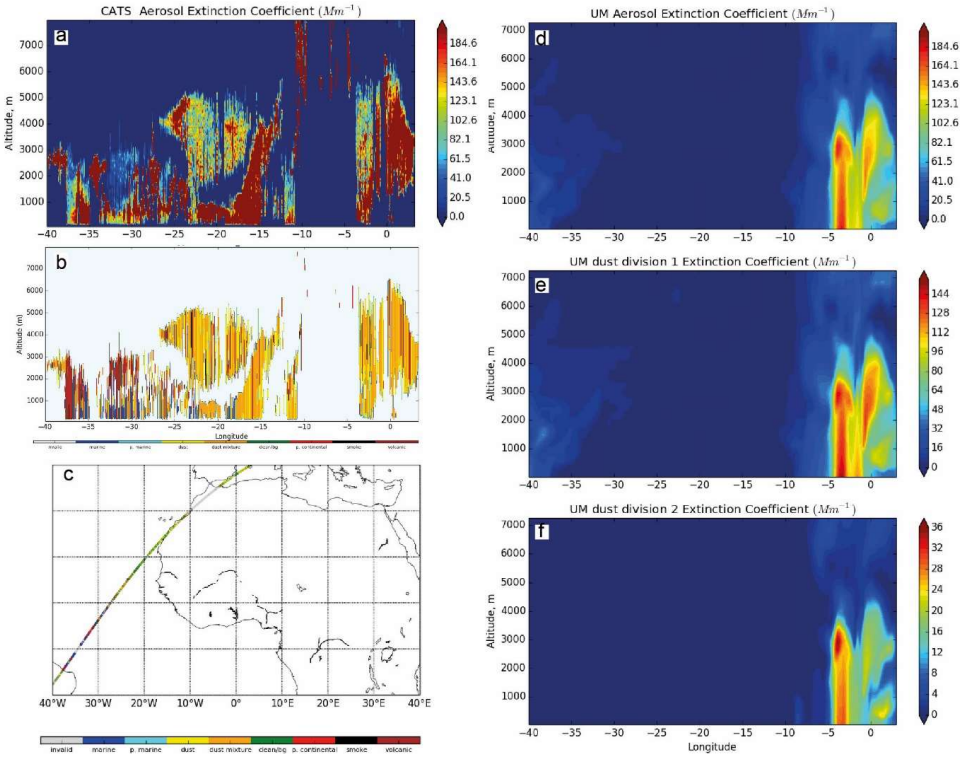

Figure 17: (a-c) CATS and (d-f) MetUM data for 18z on the 7th August, in the form of vertical cross–
975 sections along the satellite track: (a) CATS extinction coefficient; (b) CATS feature type; (c) CATS overpass track; (d) MetUM total dust extinction coefficient; (e) MetUM d1 dust extinction coefficient; and (f) MetUM d2 dust extinction coefficient. Flight B920 is simultaneous to this satellite overpass near the Cape Verde islands. Note that panel (a) may include some cloud signal (compare with panel b).

https://doi.org/10.5194/acp-2020-57
Preprint. Discussion started: 16 April 2020

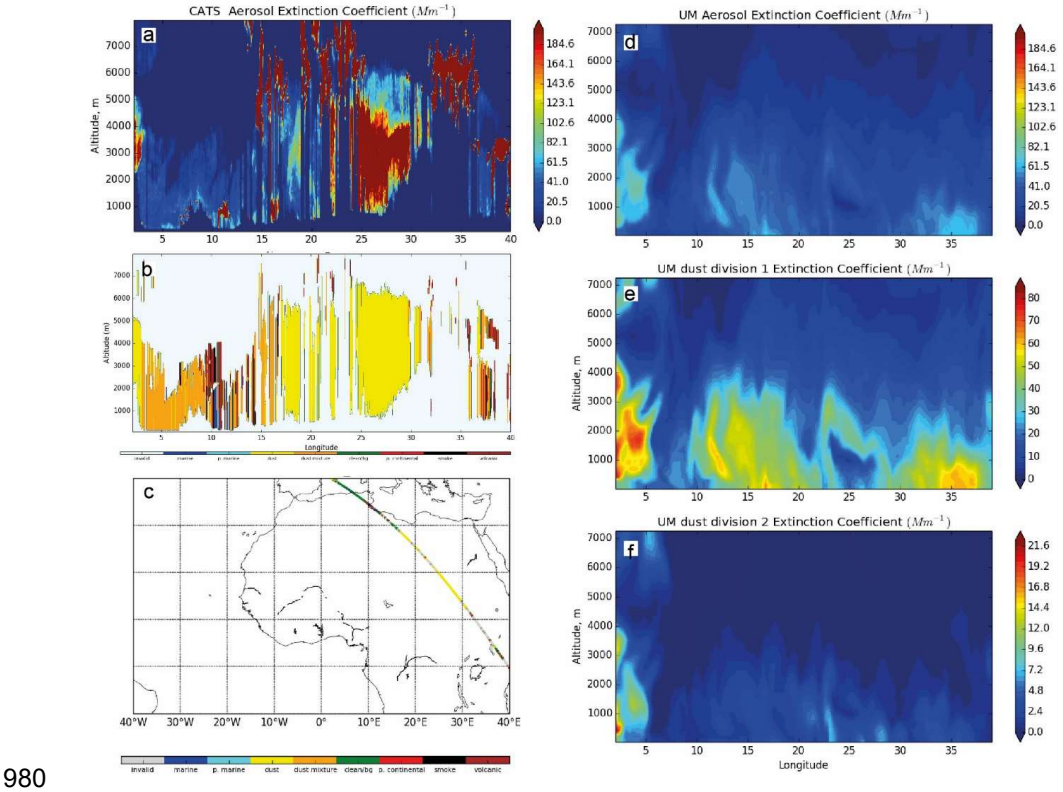

Figure 18: (a-c) CATS and (d-f) MetUM data for 00z on the 8th August, in the form of vertical cross–sections along the satellite track: (a) CATS aerosol extinction coefficient; (b) CATS feature type; (c) CATS overpass track; (d) MetUM total dust extinction coefficient; (e) MetUM d1 dust extinction coefficient; and (f) MetUM d2 dust extinction coefficient. Note that panel (a) may include some cloud signal (compare with panel b).

https://doi.org/10.5194/acp-2020-57
Preprint. Discussion started: 16 April 2020

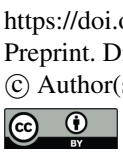

Atmospheric Chemistry and Physics Discussions

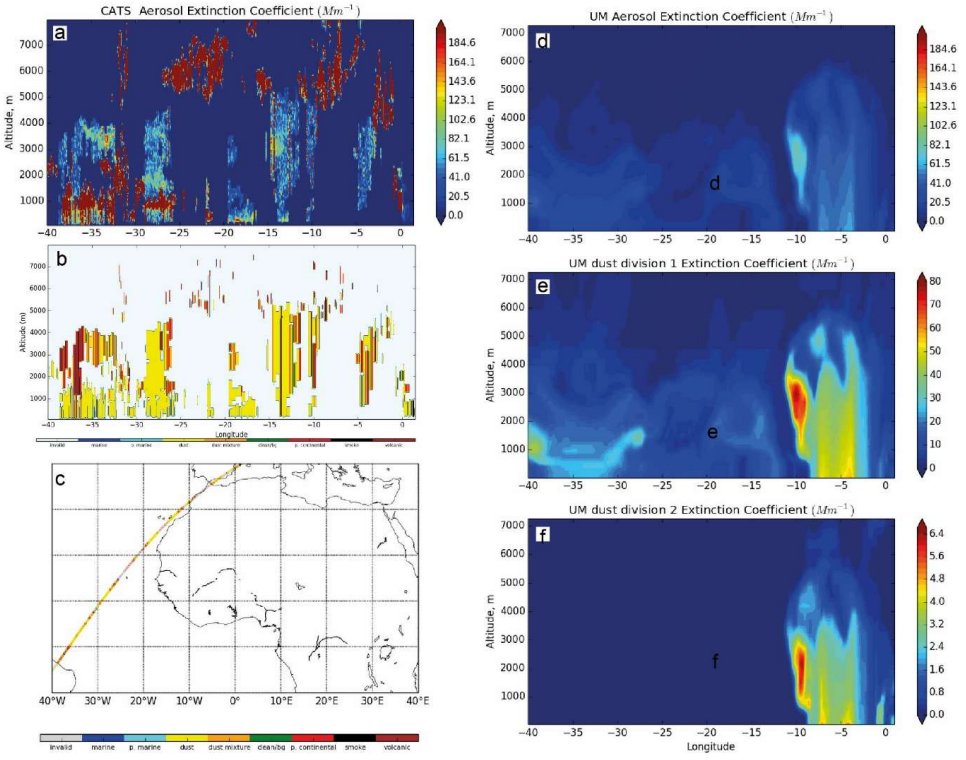

Figure 19: (a-c) CATS and (d-f) MetUM data for 00z on the 10th August, in the form of vertical cross–sections along the satellite track: (a) CATS aerosol extinction coefficient; (b) CATS feature type; (c) CATS overpass track; (d) MetUM total dust extinction coefficient; (e) MetUM d1 dust extinction coefficient; and (f) MetUM d2 dust extinction coefficient. Note that panel (a) may include some cloud signal (compare with panel b).

https://doi.org/10.5194/acp-2020-57
Preprint. Discussion started: 16 April 2020

Atmospheric Chemistry and Physics Discussions

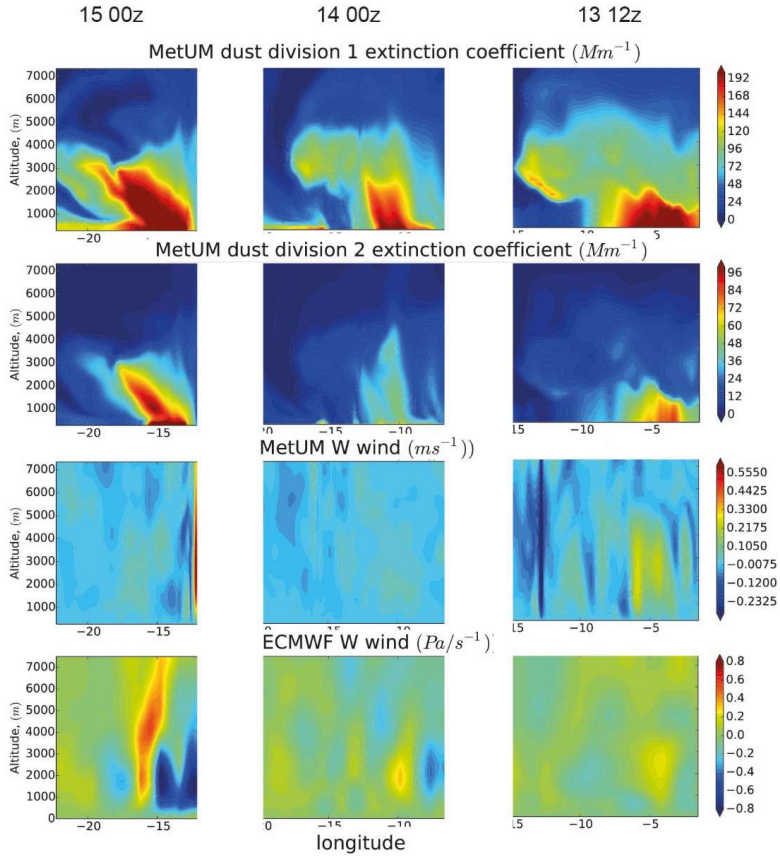

Figure 20: Contribution to the extinction coefficient by MetUM dust divisions d1 and d2 (top two rows), MetUM Westerly wind component, and ECMWF CAMS largescale wind. These cross-sections are extracted along the dust trajectory shown in fig 1, for case study 3 (flight B927, 13th August).